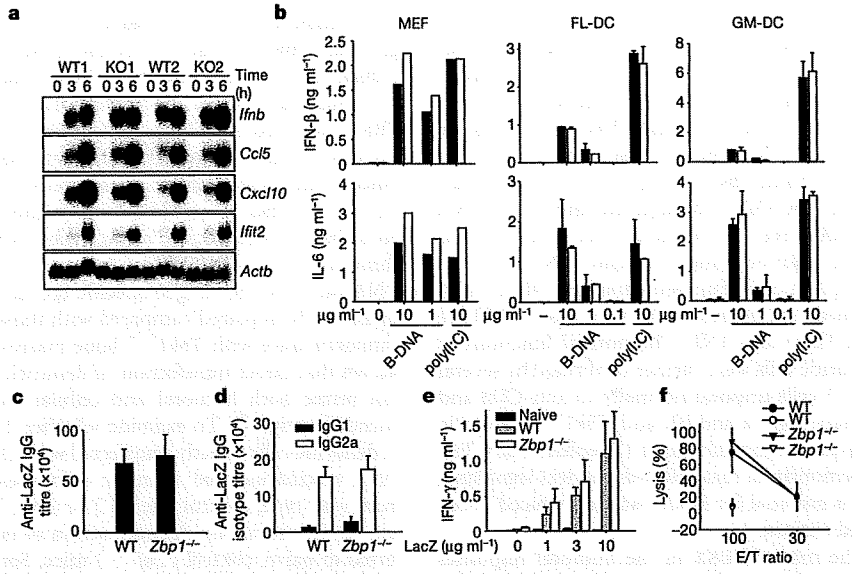

Figure 4 | Effects of ZBP1 deficiency on the innate immune activation by B-DNA and the adaptive immune responses to DNA vaccine. MEFs or bone marrow dendritic cells generated by GM-CSF (GM-DC) or Flt3 (Fms-like tyrosine kinase 3) ligand (FL-DC) were stimulated with poly(dA-dT)•poly (dT-dA) by transfection. Three and six hours later, the MEF messenger RNA expression of *Ifnb*, *Ccl5*, *Cxcl10*, *Ifit2* and *Actb* was determined by northern blot analysis (**a**), and IFN-β and IL-6 concentrations at 24 h stimulation were measured by ELISA (**b**, black bars, wild type; white bars, $Zbp1^{-/-}$). Mice lacking ZBP1 were immunized with a DNA vaccine, and two weeks after the second immunization, antigen-specific serum IgG (**c**), IgG1 and IgG2a (**d**) and IFN-γ concentration (**e**) as well as percentage lysis of the immunized mice spleen with (filled symbol) or without (open symbol) LacZ antigen (**f**) were measured. Data are the averages ± s.d. of three mice per group (except **f**, which is representative of two experiments); $^*P < 0.01$ against wild-type mice.

$CD8^+$ T cells after DNA vaccination. Wild-type, control ($Tnf^{-/-}$) and $Tbk1^{-/-}$ mice received $Tbk1^{+/+}$ or $Tbk1^{-/-}$ bone marrow cells and were immunized with a DNA vaccine. Proliferation of antigen-specific $CD4^+$ and $CD8\ T^+$ cells was analysed by a CFSE (5-(and 6-)carboxyfluorescein diacetate succinimidyl ester)-based division assay using flow cytometry. In wild-type mice immunized with DNA vaccine, a significant number of antigen-specific $CD4^+$ and $CD8^+$ T cells proliferated after five days in response to LacZ antigen (Fig. 3f). Although $Tbk1^{+/+}$ chimaeric mice with $Tbk1^{-/-}$ bone marrow displayed a comparable number of proliferating antigen-specific $CD4^+$ and $CD8^+$ T cells to $Tbk1^{+/+}$ chimaeric mice with $Tbk1^{+/+}$ bone marrow, $Tbk1^{-/-}$ chimaeric mice with $Tbk1^{+/+}$ or $Tbk1^{-/-}$ bone marrow had significantly fewer proliferating antigen-specific $CD8^+$ T cells (Fig. 3f). Interestingly, $Tbk1^{-/-}$ chimaeric mice with $Tbk1^{-/-}$ bone marrow, but not those with $Tbk1^{+/+}$ bone marrow, had significantly fewer proliferating antigen-specific $CD4^+$ T cells (Fig. 3f), suggesting that non-haematopoietic cells (or radiation-resistant cells), but not bone-marrow-derived, most probably haematopoietic cells, are required for optimal antigen-specific $CD8^+$ T-cell proliferation, whereas both are required for proliferation of $CD4^+$ T cells after DNA vaccination.

Our results revealed that the TLR9 ligand activity of plasmid DNA seems minimal for its adjuvant effects, and that the double-stranded B-form of plasmid DNA might be the critical adjuvant element for DNA vaccine, especially when introduced into the cytoplasm and/or nucleus by transfection such as electroporation. We carefully excluded possibilities that RNA generated during DNA vaccination acts as an adjuvant by activating TBK1-dependent signalling, because mice deficient for TRIF, MyD88 and IPS-1 are essential for TLR3-, TLR7/8- and RIG-I/MDA5-mediated RNA recognition, respectively, were intact in inducing DNA vaccine immunogenicity (Supplementary Figs 2 and 6). We also evaluated a possibility of ZBP1 (renamed as DAI in ref. 4 which was recently demonstrated *in vitro* as a candidate for a B-DNA receptor[4], by generating its knockout mice (Supplementary Fig. 7). The results *in vitro* and *in vivo*, however, showed that ZBP1 was not essential for either innate or adaptive responses to B-DNA or DNA vaccination, respectively (Fig. 4). Mouse embryonic fibroblasts (MEFs), two type of bone-marrow dendritic cells and macrophages responded to B-DNA and plasmid DNA as well as DNA virus infection normally to produce type-I IFNs, IL-6 and the other IFN-inducible chemokines, evaluated by northern blot, PCR with reverse transcription (RT–PCR) and ELISA (Fig. 4a, b and data not shown). In addition, ZBP1 was dispensable for inducing DNA vaccine immunogenicity including both T and B cells specific to the encoded antigen (Fig. 4c–f). Thus, ZBP1 is dispensable for both innate and adaptive immune responses to B-DNA and DNA vaccine, respectively, although its redundant role(s) is not formally excluded.

The importance of TBK1-mediated innate immune signalling for adjuvant effect, possibly through type-I IFNs, has been implicated because TRIF-dependent signalling was the major contributor to the adjuvant activity of monophosphoryl lipid A[5], and co-administration of the *Irf3*, *Irf7* or *Trif* gene as a genetic adjuvant for a DNA vaccine augmented the immunogenicity[17,27]. It will be of interest to investigate whether activation of TBK1-dependent pathway is involved in the immunogenicity of the other vaccines and to develop novel vaccine adjuvants that activate the TBK1-dependent signalling pathway. Although further studies are needed to clarify the factors including a potential DNA sensor(s) that mediates DNA-activated, TBK1-mediated innate immune activations towards adaptive immune responses or, ultimately, memory, our results may provide insights into the molecular and cellular mechanisms by which DNA vaccines trigger innate and adaptive immune responses to the encoded antigen.

METHODS SUMMARY

Mice, cells and reagents. Mutant mice lacking TNF, TBK1, IKK-i (encoded by $Ikbke^{-/-}$), TLR9, MyD88, TRIF, IFN-αβR (encoded by $Ifnr2^{-/-}$) or IPS-1, either on a 129/Ola × C57/BL6 or on a C57/BL6 background, have been described previously[20,28]. Mice lacking ZBP1 (also known as DLM-1 or DAI) were generated as described in Supplementary Fig. 7a and in the Methods. Spleen cells, MEFs and dendritic cells (GM-DCs or FL-DCs) were prepared as described previously[20]. Cells were stimulated in the presence of the indicated stimuli, and supernatants or total RNAs were collected for cytokine ELISA or for northern blot or RT–PCR, respectively, performed as described previously[20,24].

DNA vaccination. Immunization of mice (3–5 mice per group) with a DNA vaccine encoding LacZ or influenza A virus NP proteins was performed by intramuscular (i.m.) electroporation (100 μg per mouse), as described previously[17]. Mice were immunized twice, on days 0 and 28, followed by immunological assays two weeks after the second immunization unless otherwise indicated. In some experiments, splenic dendritic cells were electroporated with DNA vaccine *in vitro* and transferred intravenously into naive mice as described previously[29]. In some experiments, bone marrow was transferred approximately 1–2 months before DNA immunization as described previously[30]. All animal experiments were approved by the institutional animal care and welfare committee, and the mice were treated in accordance with the animal care guidelines of the Research Institute for Microbial Diseases, Osaka University, Japan.

Measurements of LacZ- or NP-specific immune responses. The serum anti-LacZ antibody titre was measured by ELISA as described previously[17]. A cytotoxic T lymphocyte (CTL) assay was performed as described previously[17]. Antigen (LacZ or NP)-specific IFN-γ production was analysed as described previously[17,28]. The number of Lac-Z-specific $CD8^+$ T cells was also measured using phycoerythrin (PE)-conjugated H-$2D^b$/LacZ(96–103) tetramer reagent (MBL)[28]. To analyse the proliferation of $CD4^+$ and $CD8^+$ T cells, spleen cells were stained with CFSE (Molecular Probes) and were cultured in the presence of LacZ protein (10 μg ml^{-1}) for 5 days. Spleen cells were stained with anti-CD4, anti-T cell receptor β (anti-TCRβ) and anti-CD8 antibody and analysed with a FACS Calibur instrument (BD) using CellQuest software (BD).

Statistical analysis. Differences between groups were analysed for statistical significance by the Student's *t*-test or ANOVA, using SigmaStat 3.0 software.

Full Methods and any associated references are available in the online version of the paper at www.nature.com/nature.

Received 25 October; accepted 29 November 2007.

1. Medzhitov, R. Recognition of microorganisms and activation of the immune response. *Nature* 449, 819–826 (2007).
2. Pulendran, B. & Ahmed, R. Translating innate immunity into immunological memory: implications for vaccine development. *Cell* 124, 849–863 (2006).
3. Donnelly, J. J., Ulmer, J. B., Shiver, J. W. & Liu, M. A. DNA vaccines. *Annu. Rev. Immunol.* 15, 617–648 (1997).
4. Takaoka, A. *et al.* DAI (DLM-1/ZBP1) is a cytosolic DNA sensor and an activator of innate immune response. *Nature* 448, 501–505 (2007).
5. Mata-Haro, V. *et al.* The vaccine adjuvant monophosphoryl lipid A as a TRIF-biased agonist of TLR4. *Science* 316, 1628–1632 (2007).
6. Krieg, A. M. Therapeutic potential of Toll-like receptor 9 activation. *Nature Rev. Drug Discov.* 5, 471–484 (2006).
7. Gavin, A. L. *et al.* Adjuvant-enhanced antibody responses in the absence of Toll-like receptor signaling. *Science* 314, 1936–1938 (2006).
8. Janssen, E. *et al.* Efficient T cell activation via a Toll-interleukin 1 receptor-independent pathway. *Immunity* 24, 787–799 (2006).
9. Yang, Z. Y. *et al.* A DNA vaccine induces SARS coronavirus neutralization and protective immunity in mice. *Nature* 428, 561–564 (2004).
10. Wang, R. *et al.* Induction of $CD4^+$ T cell-dependent $CD8^+$ type 1 responses in humans by a malaria DNA vaccine. *Proc. Natl Acad. Sci. USA* 98, 10817–10822 (2001).
11. Gurunathan, S., Klinman, D. M. & Seder, R. A. DNA vaccines: immunology, application, and optimization. *Annu. Rev. Immunol.* 18, 927–974 (2000).
12. Spies, B. *et al.* Vaccination with plasmid DNA activates dendritic cells via Toll-like receptor 9 (TLR9) but functions in TLR9-deficient mice. *J. Immunol.* 171, 5908–5912 (2003).
13. Babiuk, S. *et al.* $TLR9^{-/-}$ and $TLR9^{+/+}$ mice display similar immune responses to a DNA vaccine. *Immunology* 113, 114–120 (2004).
14. Tudor, D. *et al.* TLR9 pathway is involved in adjuvant effects of plasmid DNA-based vaccines. *Vaccine* 23, 1258–1264 (2005).
15. Ulmer, J. B., Wahren, B. & Liu, M. A. Gene-based vaccines: recent technical and clinical advances. *Trends Mol. Med.* 12, 216–222 (2006).
16. Widera, G. *et al.* Increased DNA vaccine delivery and immunogenicity by electroporation *in vivo*. *J. Immunol.* 164, 4635–4640 (2000).
17. Takeshita, F. *et al.* Toll-like receptor adaptor molecules enhance DNA-raised adaptive immune responses against influenza and tumors through activation of innate immunity. *J. Virol.* 80, 6218–6224 (2006).
18. Ishii, K. J. & Akira, S. Innate immune recognition of, and regulation by, DNA. *Trends Immunol.* 27, 525–532 (2006).
19. Okabe, Y., Kawane, K., Akira, S., Taniguchi, T. & Nagata, S. Toll-like receptor-independent gene induction program activated by mammalian DNA escaped from apoptotic DNA degradation. *J. Exp. Med.* 202, 1333–1339 (2005).
20. Ishii, K. J. *et al.* A Toll-like receptor-independent antiviral response induced by double-stranded B-form DNA. *Nature Immunol.* 7, 40–48 (2006).
21. Stetson, D. B. & Medzhitov, R. Recognition of cytosolic DNA activates an IRF3-dependent innate immune response. *Immunity* 24, 93–103 (2006).
22. Le Bon, A. & Tough, D. F. Links between innate and adaptive immunity via type I interferon. *Curr. Opin. Immunol.* 14, 432–436 (2002).
23. Baccala, R., Hoebe, K., Kono, D. H., Beutler, B. & Theofilopoulos, A. N. TLR-dependent and TLR-independent pathways of type I interferon induction in systemic autoimmunity. *Nature Med.* 13, 543–551 (2007).
24. Hemmi, H. *et al.* The roles of two IκB kinase-related kinases in lipopolysaccharide and double stranded RNA signaling and viral infection. *J. Exp. Med.* 199, 1641–1650 (2004).
25. Hemmi, H. *et al.* A Toll-like receptor recognizes bacterial DNA. *Nature* 408, 740–745 (2000).
26. Condon, C., Watkins, S. C., Celluzzi, C. M., Thompson, K. & Falo, L. D. Jr. DNA-based immunization by *in vivo* transfection of dendritic cells. *Nature Med.* 2, 1122–1128 (1996).
27. Sasaki, S., Amara, R. R., Yeow, W. S., Pitha, P. M. & Robinson, H. L. Regulation of DNA-raised immune responses by cotransfected interferon regulatory factors. *J. Virol.* 76, 6652–6659 (2002).
28. Koyama, S. *et al.* Differential role of TLR- and RLR-signaling in the immune responses to influenza A virus infection and vaccination. *J. Immunol.* 179, 4711–4720 (2007).
29. Ishii, K. J. *et al.* CpG-activated $Thy1.2^+$ dendritic cells protect against lethal *Listeria monocytogenes* infection. *Eur. J. Immunol.* 35, 2397–2405 (2005).
30. Kaisho, T. *et al.* IκB kinase α is essential for mature B cell development and function. *J. Exp. Med.* 193, 417–426 (2001).

Supplementary Information is linked to the online version of the paper at www.nature.com/nature.

Acknowledgements The authors thank T. Horii, K. Suzuki and S. Sasaki for suggestions, and Y. Fujita for technical support. This study was supported by Grant-in-Aid for Scientific Research (B) (to K.J.I.) from the Ministry of Education, Culture, Sports, Science and Technology in Japan.

Author Contributions K.J.I., C.C. and S.A. designed the research and analysed data. K.J.I., S.K. and C.C. performed most experiments. T.K. generated ZBP-1-deficient mice and performed the related experiments. K.M. and O.T. performed the bone-marrow-transfer experiments. S.U., T.K. and H.K. provided mutant mice. F.T. provided critical materials and advice. K.J.I., C.C. and S.A. prepared the manuscript.

Author Information Reprints and permissions information is available at www.nature.com/reprints. Correspondence and requests for materials should be addressed to K.J.I. (kenishii@biken.osaka-u.ac.jp) or S.A. (sakira@biken.osaka-u.ac.jp).

METHODS

Mice, cells and reagents. In brief, bone marrow cells were cultured in DMEM medium supplemented with 10% FCS, 100 mM 2-mercaptoethanol (2-ME) and 100 ng ml^{-1} human FLT3 ligand (PeproTech) or 10 ng ml^{-1} mouse GM-CSF (PeproTech) for 7–9 days to use as FL-DCs or GM-DCs, respectively. For liposomal transfection, DNA was mixed with Lipofectamine 2000 (Invitrogen) at a 1:1 (v/w) ratio in OptiMEM for 15 min before use in the stimulation experiments. In some experiments, splenic dendritic cells (1×10^5) were electroporated with DNA vaccine (150 μF, 300 V, BioRad) *in vitro*. Synthetic polydeoxynucleotides (B-DNA; poly(dA-dT)•(dT-dA) and poly(I:C); poly(rI)•poly(rC)) and CpG ODNA were purchased from Amersham Biosciences and Gene Design. All DNA used was tested and was free of endotoxin (<0.001 U mg^{-1} DNA).

RT–PCR. RT–PCR was performed as described previously[20]. In brief, total RNA was extracted using TRIzol reagent (Invitrogen), and then 1 μg total RNA was reverse transcribed with SuperScript II reverse transcriptase (Invitrogen) according to the manufacturer's protocol. Complementary DNA was generated by standard PCR of 28 cycles using primers as described previously.

Northern blot. MEFs were transfected with 1 μg ml^{-1} poly(dA-dT)•poly(dT-dA) for three and six hours, and total RNA was extracted using TRIzol reagent (Invitrogen). RNA was electrophorated, transferred to nylon membranes and then hybridized with the indicated cDNA probes. To detect the expression of *Zpb1* mRNA, a 372-bp fragment (503–875) was used as a probe. The same membrane was re-hybridized with a β-actin probe.

ELISA. Cell culture supernatants were collected and analysed for IFN-α, IFN-β, IFN-γ and IL-6 concentration by ELISA according to the manufacturer's protocol. ELISA kits for mouse IFN-α and IFN-β were purchased from PBL Biomedical Laboratories; those for IFN-γ and IL-6 were obtained from R&D Systems.

Measurement of serum IgG. The serum anti-LacZ antibody titre was measured by ELISA as described previously[17,28]. In brief, 96-well plates were coated with a LacZ protein at 1 μg ml^{-1} in a carbonate buffer (pH 9.6), and incubated for 18 h at 4 °C. Plates were then washed with PBS containing 0.05% Tween 20. Serial dilutions of serum in PBS/Tween containing 5% skimmed milk were applied and incubated for 2 h at room temperature. After washing, antibodies were detected using goat anti-mouse total IgG, IgG1 or IgG2a conjugated to horseradish peroxidase (Southern Biotech). After an additional washing step, the plates were stained using 3,3′,5,5′-tetramethylbenzidine (TMB, Sigma) as a substrate. The reaction was stopped with 1 M H_2SO_4 and the absorbance was measured. For serum total IgG, IgG1 and IgG2a were measured by coating the plates with anti-immunoglobulin, followed by same methods as described previously. The cut-off value was defined as the mean value of absorption of negative control serum plus two standard deviations.

Measurements of T-cell responses. Spleens were extracted 14 days after the second immunization and 5×10^5 spleen cells were seeded on 96-well plates and then stimulated with synthetic peptides (Operon) specific for LacZ (H-2D^b DAPIYTNV) or influenza A virus NP protein (I-A^b ARSALILRGSVAHKSCLPACVYGP or H-2^b ASNENMETM) at 0.1, 1 and 10 μg ml^{-1}. Seventy-two hours later, the cell culture supernatants were collected and analysed for the IFN-γ concentration by ELISA. A CTL assay was performed as described previously[17]. In brief, single-cell suspensions of spleen cells were prepared from mice 14 days after the second infection, and were seeded onto 24-well plates and cultured in RPMI complete medium in the presence of a peptide specific to NP (H-2^b; 1 μg ml^{-1}) for five days; these were then used as effector cells. Ten-thousand target EL4 cells pulsed with the same peptide were incubated with increasing numbers of effector cells for 4 h at 37 °C in 5% CO_2, and then the lactate dehydrogenase (LDH) levels in cell culture supernatants were measured according to the manufacturer's protocol (Promega). Tetramer assays for measuring NP-specific CD8 T-cell precursors were performed as described previously[17]. In brief, spleen cells were collected and incubated with H-2D^b tetramer specific to LacZ (DAPIYTNV), PE-conjugated TCRβ, allophycocyanin (APC)-conjugated CD8 and anti-CD16/32 (Fc block) for 30 min at room temperature, and then washed with PBS. Pellets were then fixed with 0.5% paraformaldehyde–PBS and analysed with FACS Calibur (Becton Dickinson) using CellQuest software (Becton Dickinson). To analyse the proliferation of CD4$^+$ and CD8$^+$ T cells, a single suspension of immunized mice spleen cells was isolated, stained with CFSE (Molecular Probes) and cultured in the presence of LacZ protein (10 μg ml^{-1}) for 5 days. Spleen cells were then collected, washed and incubated with PE-conjugated CD4, PE–Cy5-conjugated anti-TCRβ, APC-conjugated anti-CD8 antibody and anti-CD16/32 (Fc block), and were analysed as described above.

Generation of ZBP1-deficient mice. The *Zbp1* gene was isolated from genomic DNA extracted from embryonic stem cells (GSI-I) by PCR. The targeting vector was constructed by replacing a 1.6-kb fragment encoding the *Zbp1* open reading frame with a neomycin-resistance gene cassette (neo) and a herpes simplex virus thymidine kinase (HSV-TK). After the targeting vector was transfected into embryonic stem cells, G418 and gancyclovir doubly resistant colonies were selected and screened by PCR and were further confirmed by Southern blotting. Homologous recombinants were micro-injected into blastocysts from C57BL/6 female mice, and heterozygous F1 progenies were intercrossed to obtain *Zbp1*$^{-/-}$ mice.

Statistical analysis. Differences between groups were analysed for statistical significance by the Student's *t*-test or ANOVA, using SigmaStat 3.0 software.

Molecular Cell
Article

Nonself RNA-Sensing Mechanism of RIG-I Helicase and Activation of Antiviral Immune Responses

Kiyohiro Takahasi,[1,6] Mitsutoshi Yoneyama,[2,3,5,6] Tatsuya Nishihori,[1] Reiko Hirai,[2,3] Hiroyuki Kumeta,[1] Ryo Narita,[2,3] Michael Gale, Jr.,[4] Fuyuhiko Inagaki,[1] and Takashi Fujita[2,3,*]
[1]Department of Structural Biology, Graduate School of Pharmaceutical Sciences, Hokkaido University, Sapporo, Hokkaido, 060-0812, Japan
[2]Laboratory of Molecular Genetics, Institute for Virus Research
[3]Laboratory of Molecular Cell Biology, Graduate School of Biostudies
Kyoto University, Kyoto, 606-8507, Japan
[4]Department of Immunology, University of Washington School of Medicine, 1959 NE Pacific Street, H-578 Health Sciences, Box 357650, Seattle, WA 98195-7650, USA
[5]PRESTO, Japan Science and Technology Agency, 4-1-8 Honcho Kawaguchi, Saitama, 332-0012, Japan
[6]These authors contributed equally to this work.
*Correspondence: tfujita@virus.kyoto-u.ac.jp
DOI 10.1016/j.molcel.2007.11.028

SUMMARY

A DExD/H protein, RIG-I, is critical in innate antiviral responses by sensing viral RNA. Here we show that RIG-I recognizes two distinct viral RNA patterns: double-stranded (ds) and 5′ppp single-stranded (ss) RNA. The binding of RIG-I with dsRNA or 5′ppp ssRNA in the presence of ATP produces a common structure, as suggested by protease digestion. Further analyses demonstrated that the C-terminal domain of RIG-I (CTD) recognizes these RNA patterns and CTD coincides with the autorepression domain. Structural analysis of CTD by NMR spectroscopy in conjunction with mutagenesis revealed that the basic surface of CTD with a characteristic cleft interacts with RIG-I ligands. Our results suggest that the bipartite structure of CTD regulates RIG-I on encountering viral RNA patterns.

INTRODUCTION

Viral infections provoke various host responses, including early innate and subsequent adaptive immune responses. Innate responses are genetically programmed to detect a wide range of viral infections and activate a set of genes encoding humoral factors known as cytokines and chemokines. The most important cytokines in viral infection are type I interferons (IFNs), which are secreted and confer antiviral activity to the host (Joklik, 1991; Samuel, 2001). Moreover, IFN and other cytokines critically contribute to the successful activation of acquired immunity. Genomes of higher eukaryotes encode receptors for detecting pathogen molecules called pathogen-associated molecular patterns (PAMPs). Toll-like receptors (TLRs) detect PAMPs of extracellular origin either at the cell surface or in the endosome (Akira et al., 2006). TLR3, TLR7/8, and TLR9 are receptors for viral polynucleotides and trigger the production of cytokines. Unlike bacteria and fungi, viruses strictly require host cells, in which they replicate; therefore, cytoplasmic receptors to detect viral infection and subsequent replication have been hypothesized to exist since the discovery of the IFN system. Recent screening of an expression cDNA library identified an RNA helicase, RIG-I, as a cytoplasmic receptor for viral replication (Yoneyama and Fujita, 2007; Yoneyama et al., 2004).

RIG-I consists of an N-terminal *c*aspase *r*ecruitment *d*omain (CARD), a domain with the signature of DExD/H box helicase (helicase domain), and a C-terminal repression domain (RD) (Saito et al., 2007; Yoneyama et al., 2004). Functional analyses revealed that the helicase domain and RD are required for detecting viral RNA and the CARD triggers the activation of a downstream signaling cascade, including the activation of transcription factors, NF-κB, interferon regulatory factor (IRF)-3, and IRF-7. RD interacts with the helicase domain (helicase linker region) and CARD. A model is proposed that, in the absence of dsRNA, RIG-I adopts a "closed" conformation but upon binding to dsRNA changes to an "open" structure, exposing the CARD. Human and mouse genomes encode another CARD-containing helicase, termed MDA5, and a structurally related helicase without a CARD, LGP2 (Yoneyama et al., 2005). Studies in knockout mice have revealed that both RIG-I and MDA5 function as cytoplasmic sensors and are physiologically critical for antiviral defense (Gitlin et al., 2006; Kato et al., 2005, 2006). Moreover, RIG-I and MDA5 function differently in the recognition of RNA viruses (Gitlin et al., 2006; Kato et al., 2006).

IFN-inducing compounds have been extensively screened in the past, and it was shown that dsRNA, particularly the synthetic cohomopolymer poly I:C, exhibits comparative activity to viral infections (Joklik, 1991; Samuel, 2001). It has been widely accepted that dsRNA is a viral PAMP because it is normally absent in mammalian cells, due to the absence of RNA-dependent RNA polymerase. Poly I:C not only activates TLR3, but when directly introduced into the cytoplasm, preferentially activates MDA5 (Alexopoulou et al., 2001; Kato et al., 2006). Conversely, dsRNA with a nonbiased sequence, prepared by in vitro transcription and annealing, preferentially activates RIG-I (Kato et al., 2006). Recently, it was discovered that ssRNA with 5′ triphosphate (5′ppp ssRNA) is a ligand for RIG-I (Hornung et al.,

2006; Pichlmair et al., 2006). These observations suggest that RIG-I and MDA5 detect different subtypes of RNA ligands and this reflects virus-specific recognition by these helicases. Thus, it could be defined that dsRNA and 5′ppp ssRNA are recognized by innate immune sensors as "nonself" RNA, whereas "self" RNAs escape from detection due to chemical modification (Fujita, 2006). In this report, biochemical properties, including RNA binding activity, ATPase activity, and helicase activity, of recombinant RIG-I were investigated using various polynucleotides.

RESULTS

Physical Association of RIG-I with Polynucleotides

To investigate the biochemical properties of RIG-I protein, we produced human RIG-I, either the wild-type or a mutant altered in Walker's ATP binding motif (K270A), using a baculovirus system, and purified it to homogeneity. The recombinant proteins were subjected to binding assays with various polynucleotides (Figure S1). The reaction mixtures were separated by nondenaturing PAGE and sequentially stained with ethidium bromide (EtBr) and Coomassie brilliant blue (CBB) to visualize the polynucleotides and RIG-I protein, respectively. RIG-I did not bind to chemically synthesized dsDNA or ssRNA but bound to dsRNA prepared by annealing chemically synthesized complementary RNA strands (Figure 1A), confirming that RIG-I specifically binds to the dsRNA structure (Yoneyama et al., 2004). Because it was reported that dsRNA with a blunt end preferentially activates the RIG-I pathway whereas dsRNA with a 3′ overhang of two nucleotides is preferentially subjected to RNA interference (Marques et al., 2006), oligonucleotides with different end structures including blunt end and 3′ and 5′ overhangs, and oligonucleotides with or without the end phosphate group were tested (Figure 1B). All the dsRNA tested exhibited clear activity to bind the recombinant RIG-I as well as the RIG-I K270A mutant, showing that the structure of the dsRNA, not its end, is critical for physical interaction between RIG-I and dsRNA. Furthermore, the ATP-binding motif of RIG-I is dispensable for binding to dsRNA.

For comparison, 5′ppp ssRNA was similarly tested. We used 63 nucleotide ssRNA (5′pppT3-63) generated in vitro by transcription for binding to RIG-I (Figure 1C). In contrast to chemically synthesized RNA (Figure 1A, lane 5), ssT3-63 exhibited binding to RIG-I, confirming the reports (Hornung et al., 2006; Pichlmair et al., 2006). As reported, ssRNA with 5′ monophosphate failed to bind to RIG-I (Figure S2). This binding is comparable to that of dsRNA and independent of an intact ATP-binding motif (RIG-IK270A) or the presence of an unhydrolyzable ATP analog, AMP-PNP.

To examine the binding sites of dsRNA and 5′ppp ssRNA on RIG-I, a competition experiment was performed (Figure 1D). When recombinant RIG-I was subjected to an electrophoresis mobility shift assay (EMSA) using a radioactive dsRNA probe, a clear complex was detected (lane 2). Complex formation was efficiently inhibited by adding a molar excess of cold dsRNA and 5′ ppp ssRNA but not 5′-OH ssRNA (lanes 3–5), suggesting that the binding sites of dsRNA and 5′ppp ssRNA overlap.

Helicase Activity of RIG-I

RIG-I retains the structural signature of RNA helicases (Cordin et al., 2006). Although previous work demonstrated that a deletion mutant of RIG-I exhibits weak dsRNA unwinding (Marques et al., 2006), helicase activity of the full-length protein has not been shown. We examined the helicase activity of full-length RIG-I in vitro using dsRNA with a different end structure as the substrate (Figure 1E). The blunt-ended dsRNA unwound very inefficiently; however, dsRNA with a 5 nt 3′ overhang significantly unwound and that with a 3′ overhang longer than 15 nt unwound completely. The 3′ overhang is essential, because the 15 nt 5′ overhang is resistant to unwinding. Unwinding requires the hydrolysis of ATP, because AMP-PNP blocked the reaction (Figure 1F, lane 11) and RIG-I K270A is inactive for unwinding (Figure S3). Some RNA helicases act to unwind RNA/DNA duplexes in addition to dsRNA substrates (Rogers et al., 2001). We tested the unwinding of RNA/DNA duplexes and dsDNA. For comparison, substrates with the same nucleotide sequence, including a 3′ overhang, were used (Figure 1F). The dsRNA and RNA/DNA duplexes with a 3′ RNA overhang unwound with comparable efficiency, but the dsDNA was totally resistant. RNA/DNA duplexes with a 3′ DNA overhang did not unwind under the same conditions (our unpublished data). These results are consistent with RIG-I binding to 47/25cP and 47/D25cP but not to D47/D25cP or D47/25cP (Figure 1G). Although the RIG-I/substrate complex is stable in the presence of AMP-PNP, the complex dissociates by the helicase reaction in the presence of ATP (Figure 1G, lanes 2 and 3 and lanes 8 and 9).

Immunogenic Properties of Various Polynucleotides

The above results reveal the requirement for RIG-I helicase activity to be a 3′ overhang longer than 5 nt. To address the involvement of helicase activity in RIG-I-mediated signaling, we transfected dsRNA used for the helicase assay (Figures 2A and 2B). 30/25cP and 47/25cP, which are highly susceptible to unwinding by RIG-I, did not activate the virus-responsive reporter, p-55C1BLuc, whereas 25/25cP and 5-47/25cP efficiently activated the reporter gene. Likewise, an RNA/DNA duplex, 47/D25cP, which was efficiently unwound by RIG-I, failed to activate the reporter gene. 5-47/D25cP, an RNA/DNA duplex with 5′ RNA overhang, did not activate the reporter, presumably due to its low affinity to RIG-I (Figure S4). These results strongly suggest that helicase activity is reversibly correlated to the immunogenic signal triggered by RIG-I.

On the other hand, ATPase-inducing activity of oligonucleotides is positively correlated to their immunogenic activity. dsRNA and 5′ppp ssRNA, but not 5′-OH ssRNA, induced ATPase activity (Figure S5A); dsRNA with blunt end or 5′ overhang induced ATPase activity, but lower activity was induced by dsRNA with 3′ overhang (Figure S5B). dsRNA is a better ATPase inducer than RNA/DNA duplex (Figure S5C); however, ATPase induction alone may not be sufficient to activate RIG-I for signaling, because 47/25c, a dsRNA with 3′ overhang, induces ATPase significantly (Figure S5B) without signaling (Figure 2A).

To explore the structural requirement of dsRNA for immunogenic signaling in detail, dsRNA with or without an end phosphate was tested. We found that phosphorylation of one of the strands is sufficient to confer the full activity of dsRNA, whereas ssRNA with a 5′-monophosphate is inactive (Figures 2C and 2D). Because RIG-I strongly binds to dsRNA with or without

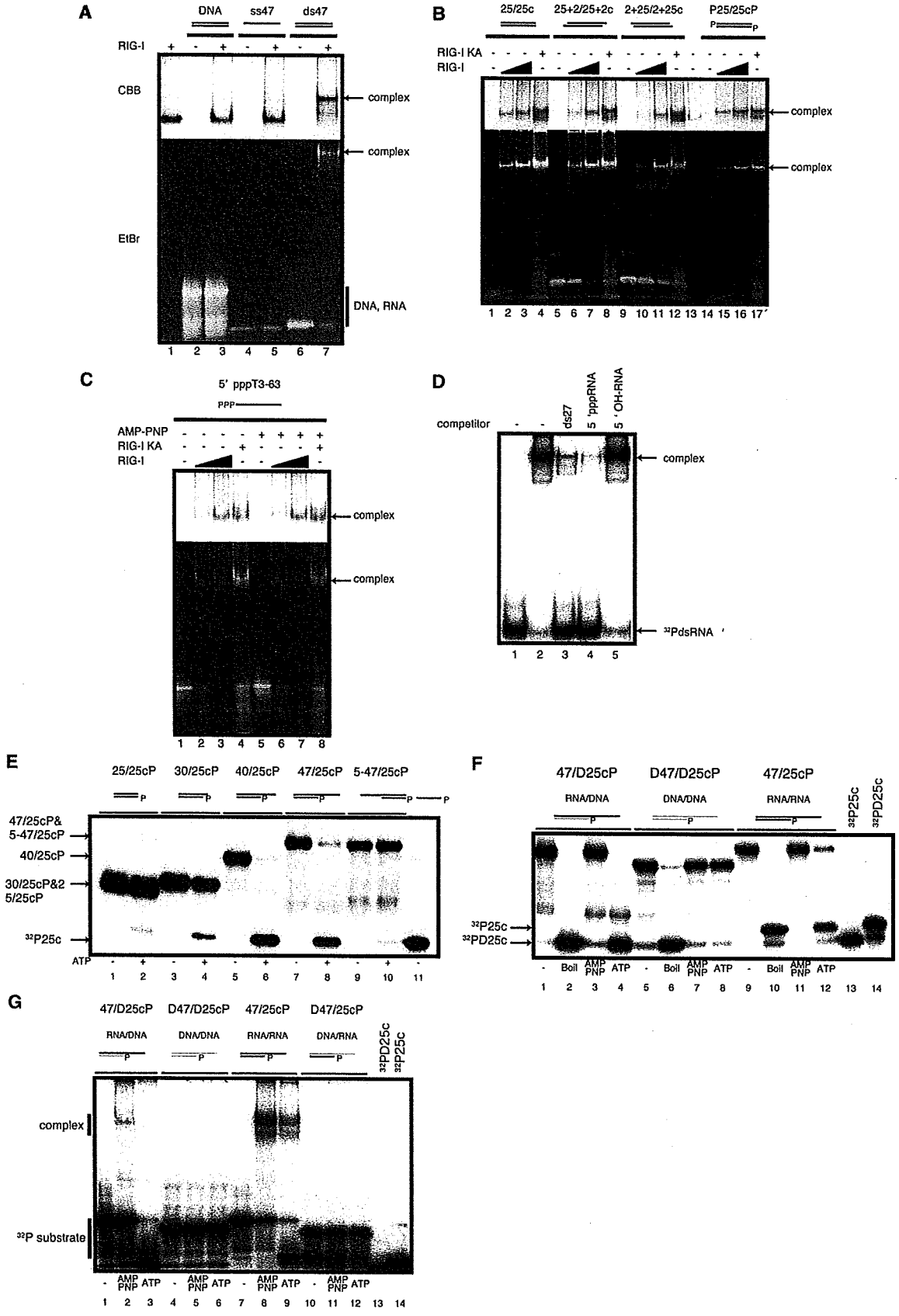
A
DNA
ss47
ds47
RIG-I
CBB
complex
complex
EtBr
DNA, RNA
1 2 3 4 5 6 7
B
25/25c
25+2/25+2c
2+25/2+25c
P25/25cP
RIG-I KA
RIG-I
complex
complex
1 2 3 4 5 6 7 8 9 10 11 12 13 14 15 16 17
C
5' pppT3-63
AMP-PNP
RIG-I KA
RIG-I
complex
complex
1 2 3 4 5 6 7 8
D
competitor
ds27
5 'pppRNA
5 'OH-RNA
complex
32PdsRNA
1 2 3 4 5
E
25/25cP
30/25cP
40/25cP
47/25cP
5-47/25cP
47/25cP&
5-47/25cP
40/25cP
30/25cP&2
5/25cP
32P25c
ATP
1 2 3 4 5 6 7 8 9 10 11
F
47/D25cP
D47/D25cP
47/25cP
RNA/DNA
DNA/DNA
RNA/RNA
32P25c
32PD25c
32P25c
32PD25c
Boil
AMP PNP
ATP
1 2 3 4 5 6 7 8 9 10 11 12 13 14
G
47/D25cP
D47/D25cP
47/25cP
D47/25cP
RNA/DNA
DNA/DNA
RNA/RNA
DNA/RNA
32PD25c
32P25c
complex
32P substrate
AMP PNP
ATP
1 2 3 4 5 6 7 8 9 10 11 12 13 14

5′-monophosphate in vitro (Figure 1B), we investigated the effect of 5′-monophosphate on dsRNA turnover in transfected cells. Figure S6 demonstrates that dsRNA possessing 5′-monophosphate at one of the strands is more stable than 5′-OH dsRNA.

RIG-I Is Required for p-dsRNA- or 5′ppp ssRNA-Induced IRF-3 Activation

To identify which of the sensing molecules is responsible for triggering the signal, p-dsRNA or 5′ppp ssRNA was transfected into wild-type MEFs and MEFs derived from *RIG-I*$^{-/-}$ mice (Figures 2E and 2F). In wild-type MEFs, all the RNA tested, including poly I:C, induced the formation of an IRF-3 dimer; however, in RIG-I-deficient MEFs, only poly I:C activated IRF-3. This result strongly suggests that p-dsRNA and 5′ppp ssRNA triggered signaling through RIG-I, whereas RIG-I is dispensable in the poly I:C-induced activation of IRF-3. The latter observation is consistent with reports that poly I:C is exclusively detected by another sensor, MDA5 (Gitlin et al., 2006; Kato et al., 2006).

dsRNA and 5′ppp ssRNA Induce Similar Conformational Change on RIG-I

The above results suggest that p-dsRNA and 5′ppp ssRNA are specifically sensed by RIG-I; however, poly I:C is distinctly recognized by RIG-I as suggested by the fact that RIG-I binds to poly I:C but is unable to trigger signaling. To explore the events following the physical association of polynucleotides with RIG-I, the complexes were subjected to limited protease digestion to monitor RIG-I conformation. We found that free RIG-I is highly sensitive to trypsin treatment and rapidly degraded (Figure 3A, lanes 1 and 2) (Saito et al., 2007); however, in the presence of dsRNA (25/25c and ds25) or 5′pppGG25, a protease-resistant 30 kDa fragment was generated (Figure 3A) and the process was facilitated in the presence of AMP-PNP (or ATP; our unpublished data). The 5′ppp moiety is critical, as 5′OH-GG25 is inactive. An essentially identical result was obtained by using chymotrypsin, showing that the observation is not due to the specificity of the protease (Figure 3A and Figure S7). These results suggest that, although structurally distinct, p-dsRNA and 5′ppp ssRNA induce similar conformational change of RIG-I upon physical interaction in the presence of AMP-PNP. Sequence analysis and reactivity to a series of monoclonal antibodies to RIG-I revealed that the 30 kDa fragment corresponds to the C-terminal region of RIG-I (our unpublished data). Remarkably, when RIG-I is bound to poly I:C it adopts a distinct conformation, as suggested by the generation of a 66 kDa, but not 30 kDa, fragment (Figure 3B and Figure S7).

RIG-I792–925(CTD) Specifically Recognizes dsRNA and 5′ppp ssRNA, and Interacts with the Helicase Linker Domain

Extensive protease treatment of the RIG-I/dsRNA complex, but not RIG-I alone, yielded a 17 kDa polypeptide (Figure S7). We hypothesized that this fragment was bound to the dsRNA and was protected from digestion. The fragment was further analyzed by mass spectrometry and protein sequencing, revealing that it corresponds to the C-terminal aa 792–925 of RIG-I (our unpublished data). A recombinant RIG-I (792–925, hereafter termed CTD) was subsequently produced in *E. coli*, and its RNA-binding properties were examined. As a control, the helicase domain (194–791), similarly produced in *E. coli*, was also tested. Figure 3C shows that dsRNA bound to RIG-I CTD, albeit with less affinity than full-length RIG-I, but not to the helicase domain. Competition experiments demonstrated that the interaction was specific to dsRNA and 5′ppp ssRNA (Figure 3C, lanes 6–12). This selective binding of RIG-I 792–925 was also demonstrated under different conditions, in which higher concentrations of unlabeled RNA were used (Figure 3D). Because the helicase domain, which catalyzes the unwinding of dsRNA, has been implicated in the binding of dsRNA (Saito et al., 2007), the identification of a distinct domain was a surprise. Furthermore, end monophosphate residue in dsRNA is not required for interaction with CTD and 5′ppp-dsRNA binds to RIG-I better than 5′ppp ssRNA, presumably due to possessing twice as many 5′ppp moieties (Figure S8). Interestingly, RIG-I CTD interacts with the RIG-I helicase linker region (420–627, Figure 3E), suggesting that this region retains the binding property of RD.

Structure of RIG-I CTD in Solution

The structure of CTD in solution was determined using NMR spectroscopy (Figure 4A, Figure S9, and Table 1). The core of the structure is formed by a β sheet comprised of six central antiparallel β strands (β3–8). Another antiparallel β sheet (β1, 2, 9) is located on top of the central β sheet and flanks α1 and α2 together with the central β sheet. The C-terminal region forms

Figure 1. RNA-Binding Properties and Helicase Activity of RIG-I

(A) Recombinant RIG-I (30 pmol) was mixed with dsDNA, synthetic 5′OH ssRNA, and dsRNA (50 pmol each) and separated. The gel was stained for nucleic acid (EtBr) and protein (CBB). Under these conditions, EtBr does not stain RIG-I and CBB does not detect oligonucleotides (data not shown).

(B) Twenty-five base pair nucleotides with different end structures (each 10 pmol) were mixed with RIG-I (30 pmol, lanes 2, 6, 10, and 15; 60 pmol, lanes 3, 7, 11, and 16) or mutant K270A (RIG-IKA; 60 pmol, lanes 4, 8, 12, and 17) and resolved by gel electrophoresis as in (A).

(C) RIG-I was mixed with 5′ppp ssRNA in the absence or presence of AMP-PNP and analyzed as in (B). Lanes 2 and 6, 30 pmol RIG-I; lanes 3 and 7, 60 pmol RIG-I; lanes 4 and 8, 60 pmol RIG-IKA.

(D) EMSA using ^{32}P-dsRNA (ds27, 0.08 pmol) as a probe. For binding competition, indicated unlabeled RNAs (500-fold molar excess over the probe) were included.

(E) RNA-unwinding activity of RIG-I. Indicated RNA substrates were analyzed for helicase activity. The reaction was run in the absence (lanes 1, 3, 5, 7, and 9) or presence (lanes 2, 4, 6, 8, and 10) of ATP. Unannealed ^{32}P-p25c was run similarly (lane 11).

(F) RNA/DNA duplex-unwinding activity of RIG-I. Indicated nucleotide duplexes along with dsRNA substrates were analyzed as in (E). Substrate alone, lanes 1, 5, and 9; boiled substrate, lanes 2, 6, and 10; reaction with AMP-PNP, lanes 3, 7, and 11; reaction with ATP, lanes 4, 8, and 12. Unannealed ^{32}P-p25c and pD25c were electrophoresed in lanes 13 and 14, respectively.

(G) EMSA of helicase reaction mixture. Helicase reaction mixtures without competitor RNA were analyzed by native PAGE. Substrate alone, lanes 1, 4, 7, and 10; reaction with AMP-PNP, lanes 2, 5, 8, and 11; reaction with ATP, lanes 3, 6, 9, and 12. Unannealed ^{32}P-p25c and pD25c are electrophoresed in lanes 13 and 14, respectively. Positions of ^{32}P-substrate and RIG-I-substrate complex are indicated.

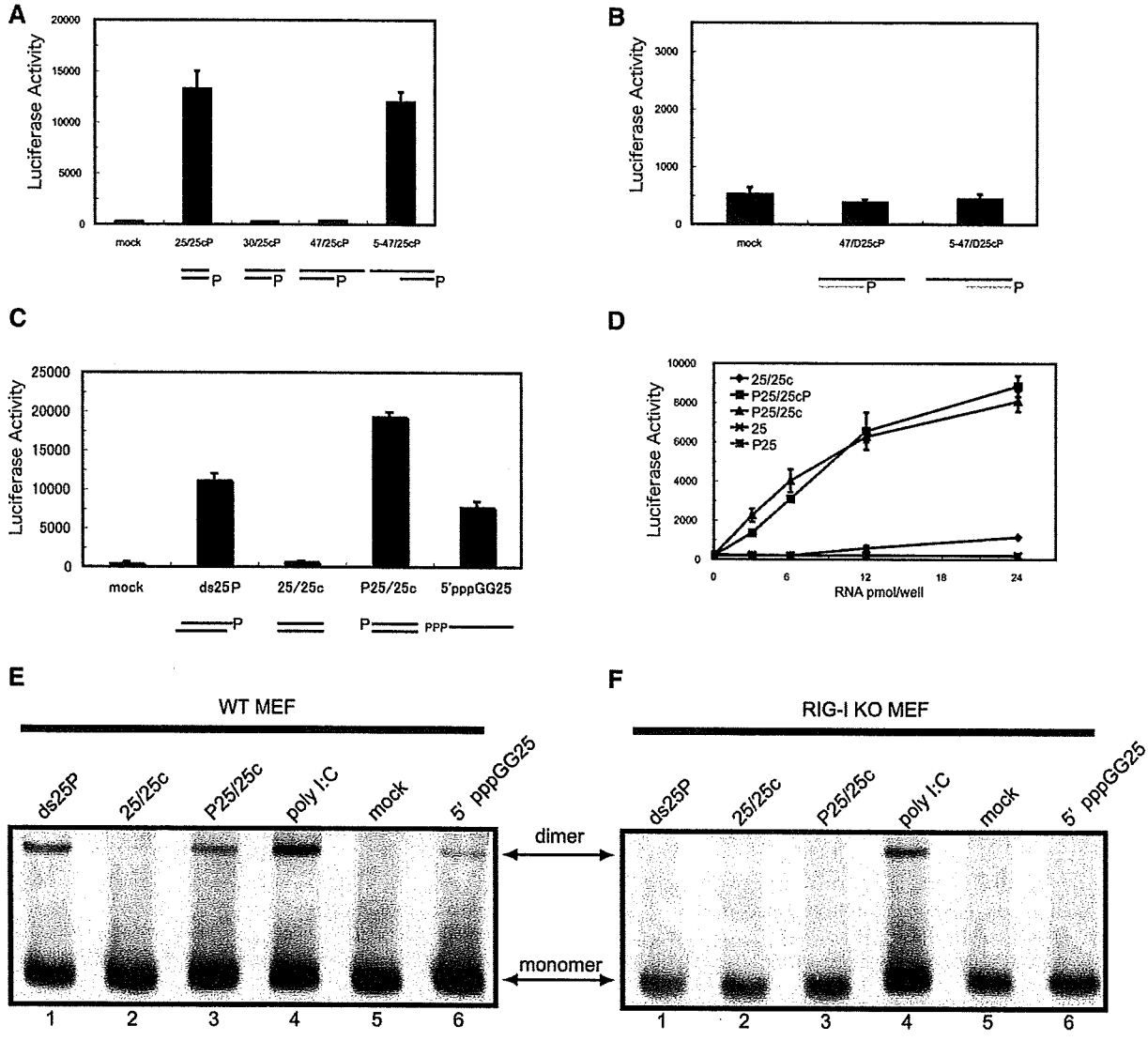

Figure 2. Gene Activation Properties of dsRNA and 5′ppp ssRNA

(A) dsRNA with a 3′ or 5′ overhang was transfected (90 pmol/3 cm dish) into L929/C1B-Luc cells, and luciferase activity derived from an integrated virus-responsive reporter gene was analyzed. RNA/DNA duplexes (B), dsRNAs with various end structures, and 5′ppp ssRNA (C) were similarly analyzed for their potential to activate virus-responsive promoter (30 pmol/well in a 12-well plate). Effect of end phosphorylation on immunogenic activity of dsRNA was analyzed (D). The values are the means ± SD from triplicate experiments. MEFs derived from wild-type mouse (WT MEF) (E) or *RIG-I*$^{-/-}$ mouse (F) in a 3 cm dish were transfected with the indicated RNA (90 pmol) and analyzed for IRF-3 dimerization.

a long unwound structure, capping one end of the central β sheet with two α helices (α3, 4) (Figure 4B). The structure is maintained by hydrophobic interactions derived from residues on the surface of those secondary structures that are well conserved among its homologs, MDA5 and LGP2 (Figure 4B). The electrostatic surface revealed that RIG-I CTD has a large basic cleft parallel to the central β sheet (Figure 4C). One edge of the cleft is capped by two α helices (α2 and α3), and the other is capped by a flexible loop between β5 and β6. In contrast, the opposite surface of CTD contains acidic patches.

Despite poor sequence homology, RIG-I CTD is structurally similar to the mammalian suppressor of Sec4 (Mss4) according to searches using Dali (Figure 4D) (Holm and Sander, 1993). Mss4 is a guanine nucleotide exchange factor (GEF) essential for the activation of Rab family GTPases (Yu and Schreiber, 1995a, 1995b). Although the central β sheet and the capping three antiparallel β strands and two α helices were conserved in both structures, there are appreciable structural differences between them (Figure 4D). RIG-I CTD lacks the βA and β hairpin (βE, βF, and a connecting loop) in Mss4. The β hairpin covers the surface of the central β sheet and is involved in binding to Rab GTPase. In contrast, RIG-I CTD has a long C-terminal tail comprised of α3, α4, and a linker that surrounds the central β sheet. RIG-I CTD also has a long flexible loop between β5 and β6. Mss4 is known to have two CysXXCys motifs that act as a Zn^{2+}-binding site, thus stabilizing the structure. The first motif

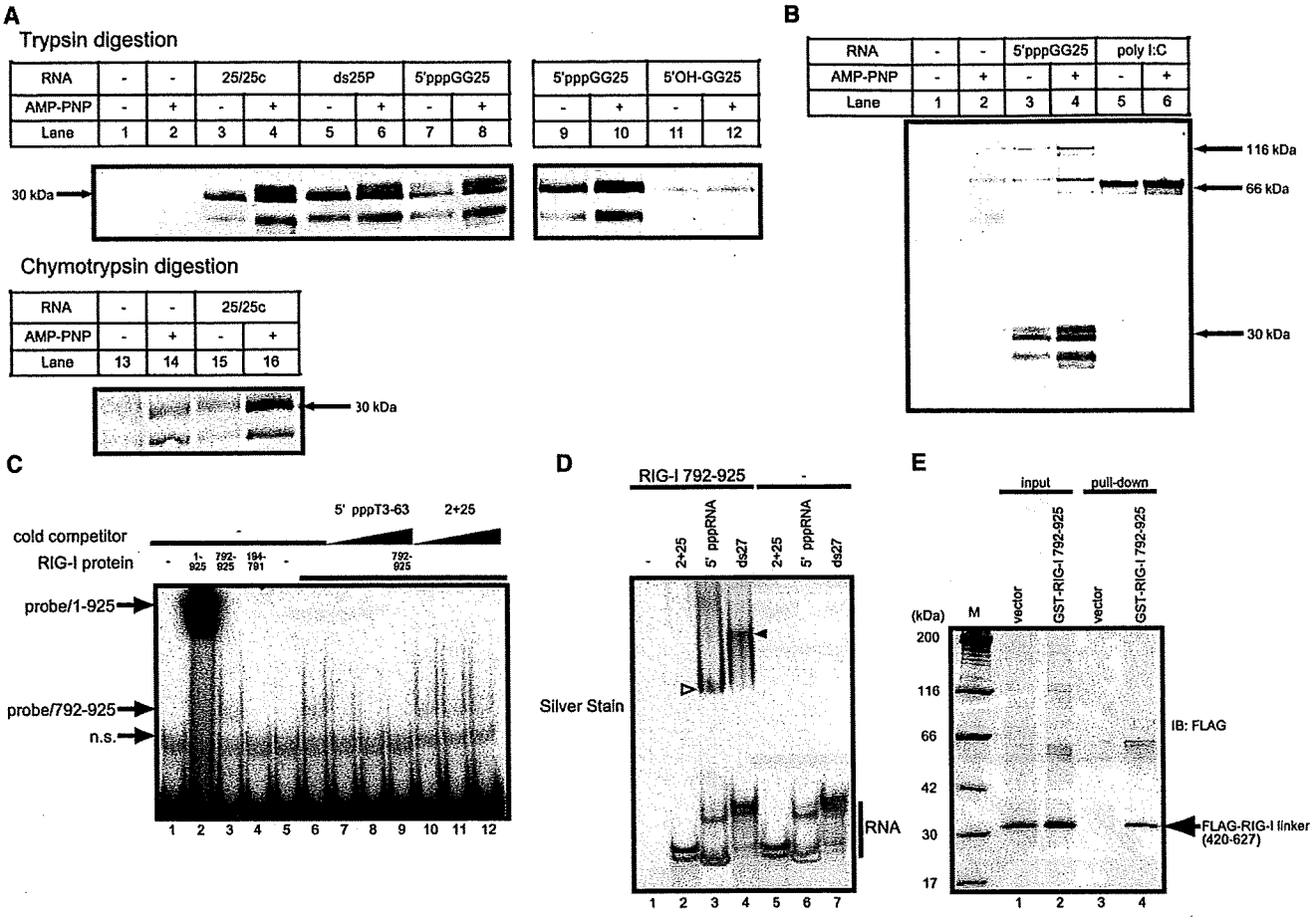

Figure 3. Conformational Change of RIG-I and Identification of CTD as the RNA Recognition Domain

(A) Protease digestion of RIG-I. RIG-I was incubated with the indicated RNA in the absence (odd number lanes) or presence of AMP-PNP (5 mM, even number lanes). The mixture was digested with trypsin (lanes 1–12) or with chymotrypsin (lanes 13–16). The digested RIG-I was analyzed by SDS-PAGE followed by anti-RIG-I immunoblotting.

(B) RIG-I was incubated with 5′ppp-GG25 or poly I:C and analyzed as in (A).

(C) Specific recognition of dsRNA and 5′ppp ssRNA by RIG-I 792–925. EMSA using a ^{32}P-labeled dsRNA probe (^{32}P-GG25/2+25c, 0.08 pmol) and either a full-length RIG-I (1–925, 30 pmol), or the C-terminal (792–925, 50 pmol) or helicase domain (194–925, 50 pmol) of RIG-I. Cold 5′ppp ssRNA (T3-63, lanes 7–9: 50, 100, and 200 pmol, respectively) or 5′OH ssRNA (ss2+25, lanes 10–12: 50, 100, and 200 pmol, respectively) was included. RIG-I/probe complexes are indicated. n.s., nonspecific band.

(D) RIG-I (792–925, 50 pmol) was mixed with 5′OH ssRNA (2+25, 100 pmol, lane 2) or 5′ppp ssRNA (T3-63, 100 pmol, lane 3) or dsRNA (ds27, 100 pmol, lane 4) and resolved in a 7.5% acrylamide gel and silver stained. The probe alone was electrophoresed as indicated (lanes 5–7). Triangles indicate RNA-protein complexes. Under these conditions, RIG-I (792–925) did not enter the gel (lane 1).

(E) Huh7 cells were transfected with the expression vector for Flag-RIG-I linker (420–627) and empty GST vector (lanes 1 and 3) or the expression vector for GST-RIG-I 792–925 (lanes 2 and 4). Cell extracts were subjected to pull-down assays using glutathione Sepharose beads and analyzed for immunoblotting (lanes 3 and 4) along with one-tenth the amount of crude extract (lanes 1 and 2, input) using anti-Flag. The position of the Flag-RIG-I linker is indicated.

is conserved in the RIG-I family, but the second motif has an insertion in RIG-I and a deletion in MDA5 (Figure 4B). We tested by atomic absorption spectrophotometer whether the solution structure of RIG-I CTD contains Zn^{2+} and found that RIG-I CTD roughly contains an equimolar amount of Zn^{2+} (Table S1). We compared the spectra with and without 50 mM EDTA (0.1 mM CTD, at 4°C for 7 days); however, negligible chemical shift perturbation was observed. On the other hand, Zn^{2+} was removed under denaturing condition (6 M guanidine hydrochloride) in the presence of 50 mM EDTA, as confirmed by atomic absorption experiments, suggesting that Zn^{2+} is involved in the structural integrity (Table S1).

Effect of Binding RNA on NMR Spectra

In order to investigate the binding surface for dsRNA, ssRNA, and 5′ppp ssRNA, NMR titration was performed with RNAs used in EMSA. A progressive decrease in intensity was observed in ^{1}H-^{15}N-HSQC spectra with the addition of either dsRNA or 5′ppp ssRNA (Figures 5A and 5B). A smaller decrease in intensity was also seen on titration with ssRNA. This indicates that the

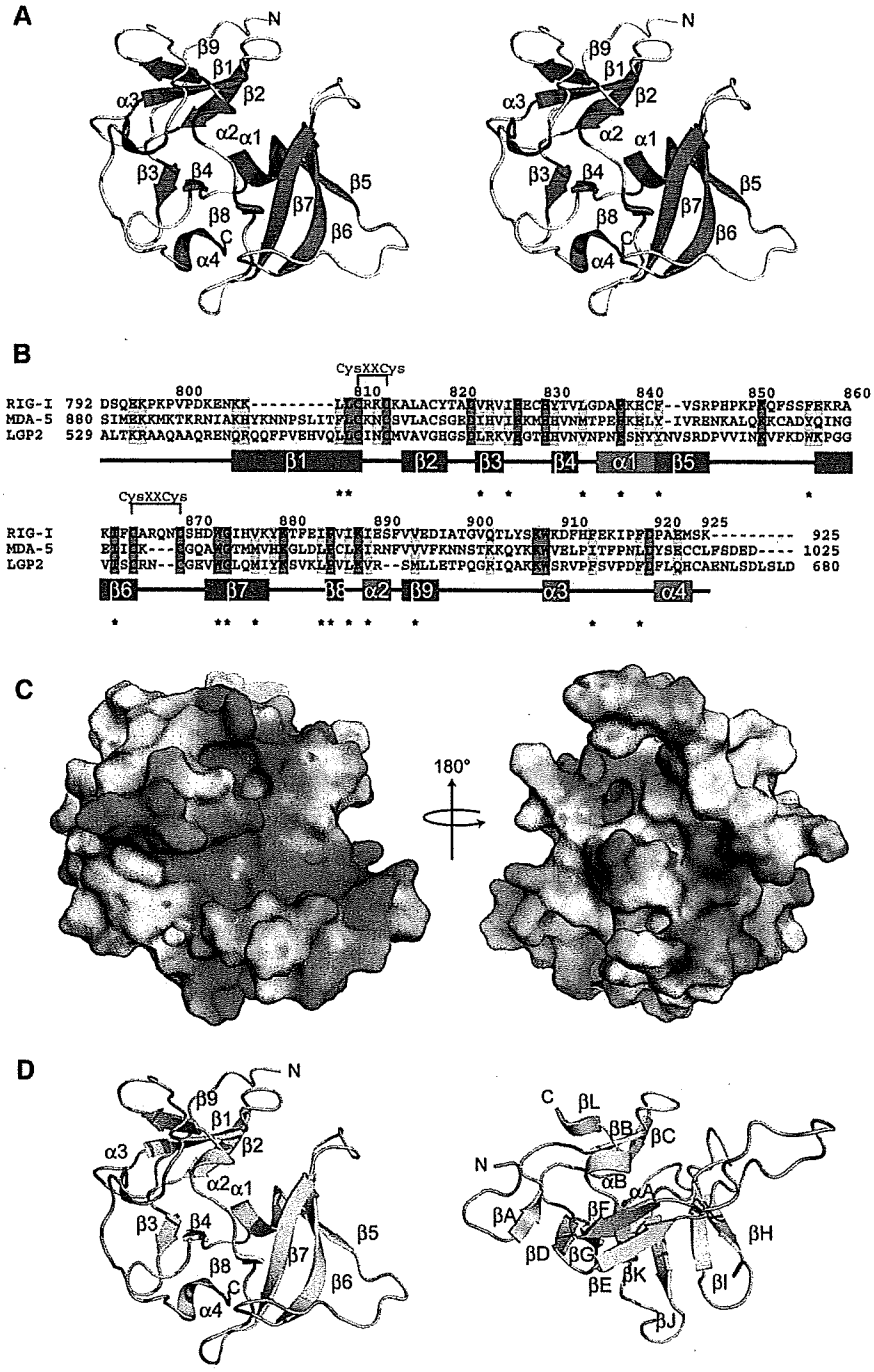

Figure 4. Structure of RIG-I CTD in Solution

(A) Stereo view of a ribbon diagram of the lowest-energy structure. Secondary structural elements are labeled.

(B) Sequence alignment of RIG-I CTD and its homologs human MDA5 and human LGP2. The secondary structural elements are indicated below the alignment. The amino acid in red and yellow indicates conserved and type-conserved residues, respectively. Conserved residues that participate in the hydrophobic core are indicated with asterisk (*). CysXXCys motifs are also indicated.

(C) The electrostatic surface potential of RIG-I CTD. Positive and negative electrostatic surfaces are in blue and red, respectively. Left, the model corresponds to the orientation of RIG-I CTD in (A). Right, surface potential of CTD rotated 180° along the vertical axis.

(D) Comparison of the structure of RIG-I CTD (left) and Mss4 (right). Structures are represented by a ribbon diagram. The structurally similar region between RIG-I CTD and MSS4 is shown in cyan, and other regions are shown in yellow. All of the figures were prepared using PyMOL (http://www.pymol.org).

formation of the protein/RNA complex is an intermediate exchange process on the NMR chemical shift timescale. The residues that disappeared were located on one surface of the protein, whereas the residues forming the opposite surface did not disappear, suggesting that the former residues participate in interaction with RNAs.

In dsRNA titration experiments, signals corresponding to the residues involved in a large cleft disappeared at 0.5 equivalents (molar ratio to RIG-I CTD). The cleft comprised β6 (Lys858 and Lys861), β7 (Asp872, Trp873, and Ile875), α2 (Ile889 and Glu890), and a flexible loop between β5 and β6 (Phe853 and Phe856). Notably, Lys858 and Lys861 are not conserved in RIG-I homologs, indicating that MDA5 and LGP2 would recognize viral RNAs in different ways. Other peaks, corresponding to Ile826 and Tyr879, also disappeared (Figure 5C). This cleft corresponds to the large basic cleft on the surface of RIG-I CTD (Figure 4C).

Surprisingly, titration with 5′ppp ssRNA showed a faster progressive decrease in intensity. Peaks responsible for binding with dsRNA also disappeared, such as β6 (Lys858, Ala860, and Lys861), β7 (Asp872, Trp873, Gly874, Ile875, His876, and Val877), α2 (Ile889 and Glu890), and the flexible loop between β5 and β6 (Phe853 and Phe856). In addition, residues on the adjacent surface formed by β4 (Tyr831), α2, and the loops between β3 and β4 (Ile826, Glu827, and His830), β7 and β8 (Tyr879), and the C-terminal tail containing α3 and α4 (Ser906, Trp908, and Lys915) disappeared with the addition of 0.25 equivalents of 5′ppp ssRNA. Residues Ala817, Val843, Arg845, Ile884, and Val893 also disappeared (Figure 5D).

These results imply that RIG-I CTD uses the large basic cleft along with the peripheral residues to recognize 5′ppp ssRNA and dsRNA. It is worth noting that the flexible loop between β5 and β6, which resides at one edge of the cleft, is conserved in MDA5 and LGP2. Likewise, residues Tyr831, Trp873, Gly874, Ile887, Lys888, Lys907, and Trp908, which reside at the other end of the cleft, are also conserved (Figures 4B and 5E).

Table 1. Structural Statistics for 20 RIG-I CTD

NOE distance constraints	
Total	2366
Short range $\|i-j\| \leq 1$	1342
Medium range $1 < \|i-j\| < 5$	271
Long range $\|i-j\| \geq 5$	753
Dihedral angle constraints	
phi	79
psi	83
Residual NOE violations	
Number > 0.3	2
Maximum (Å)	0.33
Residual angle violations	
Number > 5.0°	0
Ramachandran statistics (%)	
Residues in most favored regions	73
Residues in additional allowed regions	26.2
Residues in generously allowed regions	0.5
Residues in disallowed regions	0.2
Structural coordinates rmsd (Å) (residues 806–845, 860–915)	
Backbone atoms for the final ensemble	0.63
All heavy atoms for the final ensemble	1.15

Effect of Amino Acid Substitutions on the Function of RIG-I CTD

To confirm the involvement of the CTD cleft in the recognition of nonself RNA, a series of point mutants in the context of full-length RIG-I were generated, expressed in 293T cells, and subjected to RNA-binding assays (Figures 6A and 6B). The wild-type and mutant RIG-I tested were produced at comparable levels in 293T cells (our unpublished data). Binding to dsRNA was not affected by K849A, whereas it was significantly impaired by the KK858/861AA mutation at the bottom of the cleft. A mutation at one edge of the cleft, KK888/907AA, also inactivated dsRNA binding. KK878/880AA, which is distal from the cleft, caused partial inhibition of dsRNA binding. Interestingly, a similar result was obtained for binding with 5′ppp ssRNA. These results not only confirm the importance of the basic cleft but also suggest the involvement of a larger surface for the recognition of nonself RNA species.

Next, we assessed the signaling function of RIG-I mutants by adding them back to *RIG-I*$^{-/-}$ MEFs and stimulating these cells with dsRNA or 5′ppp ssRNA (Figures 6C and 6D). Consistent with the RNA-binding properties of the mutants, KK858/861AA and KK888/907AA are incapable of complementing RIG-I function, whereas R849A, which normally recognizes ligand RNAs, efficiently restored RIG-I's function. The partial RNA-binding mutant KK878/880AA partially retained reactivity to dsRNA and 5′ppp ssRNA. In summary, the results of mutagenesis are consistent with our hypothesis that the basic cleft is responsible for the recognition and triggering of antiviral signaling. It is worth noting that although RIG-I CTD interacts with the helicase linker region (Figure 3E), none of the RNA binding-deficient mutants exhibited constitutive activation of the signal, suggesting that the RNA-sensing surface of CTD is independent of the RD function.

Finally, we investigated the binding properties of poly I:C and RIG-I. RIG-I was subjected to EMSA using ^{32}P-labeled poly I:C as a probe, and binding was competed by a 1600-fold molar excess of various cold RNA (Figure 6E). Although efficient competition was observed with poly I:C, short dsRNA or 5′ppp ssRNA failed to exhibit competition under these conditions. When ^{32}P-labeled short dsRNA was used as a probe, poly I:C efficiently competed binding (Figure 6F). These results suggest that poly I:C, short dsRNA, and 5′ppp ssRNA bind with RIG-I at overlapping sites but poly I:C exhibits significantly higher affinity. We hypothesized that poly I:C interacts with an additional site on RIG-I, presumably with the helicase domain. There are several conserved motifs within the helicase domain, such as TAS (amino acid residues 409 to 410), which is implicated in the unwinding reaction (Pause and Sonenberg, 1992). EMSA was performed using wild-type RIG-I and a mutant of the TAS motif (TS409/411AA) using ^{32}P-labeled poly I:C or short dsRNA (ds25/25c) (Figure 6G). Disruption of the TAS motif apparently impaired binding with poly I:C, whereas binding with short dsRNA was unaffected, suggesting that poly I:C interacts with additional sites, including the TAS motif of the helicase domain.

DISCUSSION

RNA-Binding and Helicase Activity of RIG-I

We produced a full-length recombinant RIG-I, purified it to homogeneity, and subjected it to biochemical analyses. First, we found that dsRNA and 5′ppp ssRNA bound to RIG-I in a competitive manner; however, binding to dsDNA or 5′OH ssRNA was undetectable. Our analysis revealed that dsRNA, relatively small in size, binds to RIG-I independent of a phosphorylated structure or overhang. By contrast, with 5′ppp ssRNA, the 5′ppp structure is critical for recognition, as dephosphorylated or chemically synthesized 5′OH ssRNA failed to bind to RIG-I (Figure 1) (Hornung et al., 2006; Pichlmair et al., 2006). Furthermore, ssRNA with 5′ mono- or diphosphate (including commercial poly rA, which was synthesized by ADP and polynucleotide phosphorylase) does not bind to RIG-I (Yoneyama et al., 2004 and Figure S2).

As predicted from its primary structure, we confirmed that RIG-I is a ligand-dependent ATPase. ATPase activity is induced by binding with various dsRNAs, including poly I:C; however, ATPase activity per se is not perfectly correlated with IFN-inducing signaling. Poly I:C does not activate RIG-I in vivo, and a particular p-dsRNA, 47/25c, induces ATPase efficiently (Figure S5) but failed to activate RIG-I to activate the IFN promoter (Figure 2A).

RIG-I exhibits apparent helicase activity toward dsRNA and RNA/DNA duplexes with a 3′ RNA overhang, indicating a clear structural requirement, the 3′ RNA overhang. RNAs with a blunt end or 5′ overhang were resistant to unwinding by RIG-I. Previously, an opposite result was reported that blunt-end RNA is a better substrate for RIG-I helicase and efficiently induces IFN in cells (Marques et al., 2006). This discrepancy is likely due to the use of a truncated RIG-I and nonoptimal assay conditions that led to inefficient unwinding. Using a series of dsRNAs, which differ in their susceptibility to unwinding by RIG-I, we found a reverse correlation between IFN-inducing potential upon the transfection of cultured cells and susceptibility to unwinding. As in vitro binding suggests (Figure 1G), this is presumably

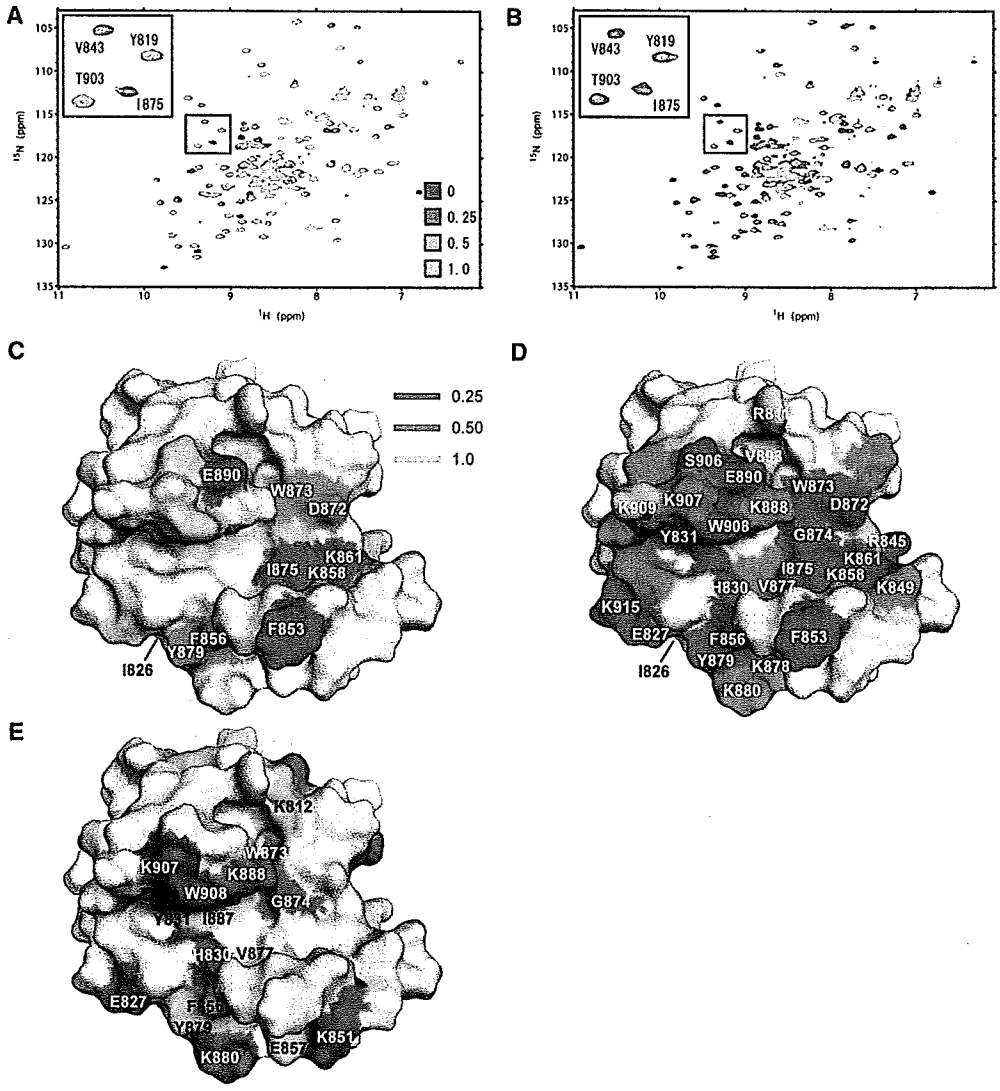

Figure 5. NMR Titration of RIG-I CTD

(A and B) NMR titration of RIG-I CTD with (A) GG25/2+25C and (B) 5′pppGG25. An overlay of ^{1}H-^{15}N-HSQC spectra is shown in blue at 0 equivalents (molar ratio of RNA to RIG-I CTD) and in yellow at 0.5 equivalents. The insert shows additional spectra at 0.25 equivalents in magenta and 1.0 equivalent in cyan. Signal intensity was normalized using the signal derived from the GST tag.

(C) dsRNA-binding site of RIG-I CTD determined from the NMR titration. Residues whose peaks on the spectrum disappeared at 0.25, 0.5, and 1.0 equivalent are shown in blue, sea blue, and light blue, respectively. Residues that disappeared with the addition of 0.5 equivalent of RNA are labeled.

(D) 5′ppp ssRNA-binding site of RIG-I CTD. The same colors as in (C) were used. Residues that disappeared with the addition of 0.25 equivalent of RNA and Lys and Arg residues that disappeared with up to 1 equivalent molar of RNA are labeled.

(E) The conserved residues are colored on the surface of RIG-I CTD. Residues completely conserved among RIG-I, MDA5, and LGP2 are in red, whereas type-conserved residues are in yellow.

because good helicase substrates readily unwound and the RIG-I/dsRNA complex is not stable in cells, whereas the resistant dsRNA/RIG-I complex may exist stably in cells to facilitate persistent interaction with interferon promoter stimulator-1 (IPS-1). The RNA/DNA duplex 47/D25cP, which possesses a 3′ overhang, is unwound by RIG-I as efficiently as the dsRNA substrate (Figure 1F); however, its 5′ overhang variant, 5-47/D25cP, was incapable of inducing IFN gene expression (Figure 2B). This is partly explained by the knowledge that 5-47/D25cP does not exhibit appreciable binding to RIG-I (Figure S4).

Although it has been proposed that large dsRNA is required to efficiently induce the production of IFN (Joklik, 1991), when transfected into cultured cells, dsRNA as small as 25 bp, possessing a 5′- or 3′-monophosphate, efficiently triggered the production. Because the 5′-monophosphate did not enhance the physical association between dsRNA and RIG-I in vitro (Figure 1B and Figure S8), or resultant conformational change, we do not know the mechanism underlying the requirement for the end monophosphate. A transfection experiment (Figure S6) suggested that an end monophosphate may enhance the stability of dsRNA in cytoplasm.

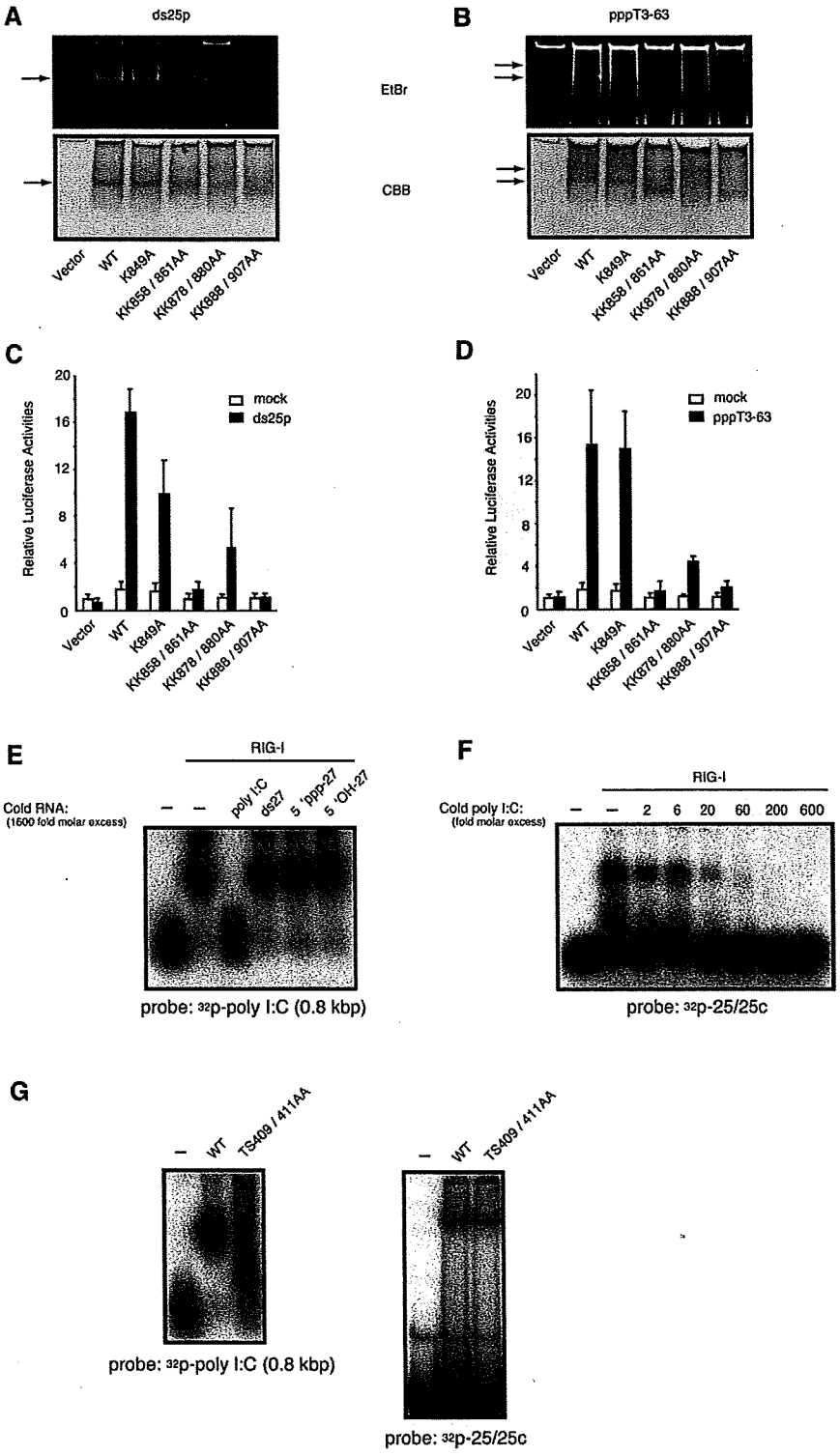

Figure 6. Functional Analysis of the Basic Surface of RIG-I CTD

(A and B) RNA-binding activity of RIG-I and its mutants. Wild-type and indicated mutants were expressed in 293T cells and purified with anti-Flag beads. Proteins were incubated with ds25p (A) or pppT3-63 (B) RNA and subjected to native PAGE. Bound RNA and protein were detected by staining with EtBr (upper panel) and CBB (lower panel), respectively. Although the protein band is smeared, clear RNA-protein complexes were detected (arrows).

(C and D) Activation of wild-type RIG-I and mutants by dsRNA and 5′ppp ssRNA. MEFs derived from *RIG-I*$^{-/-}$ mice were transfected with the reporter gene, p-55C1BLuc, and pRL-tk, together with the expression vector for RIG-I and mutants. Cells were stimulated by transfection with ds25p (C) or pppT3-63 (D) and subjected to a dual-luciferase assay. The values are the means ± SD from triplicate experiments.

(E) EMSA of recombinant RIG-I (10 pmol) using ^{32}P-poly I:C (2.5 fmol) in the absence or presence of indicated cold RNA (each 1600-fold molar excess over probe).

(F) EMSA of recombinant RIG-I (10 pmol) using ^{32}P-25/25c (10 fmol) in the absence or presence of indicated molar excess of cold poly I:C.

(G) Wild-type and TS409/411AA mutant of RIG-I were produced in 293T cells and purified as described in the Experimental Procedures and subjected to EMSA using ^{32}P-poly I:C (left) or ^{32}P-25/25c (right) as probes.

Conformational Change of RIG-I Induced by Binding with Ligand RNA Species

dsRNA and 5′ppp ssRNA recognize overlapping sites on RIG-I and induce similar conformational change, as demonstrated by digestion with trypsin or chymotrypsin. ATP (or AMP-PNP) significantly enhances the conformational change triggered by dsRNA or 5′ppp ssRNA; however, ATP per se is not sufficient to initiate the reaction (Figure 3A). This is consistent with the observation that mutant RIG-I with a disrupted ATP-binding motif (K270A) is incapable of transmitting a signal, although its binding activity to dsRNA and 5′ppp ssRNA is unaffected (Figures 1B and 1C).

CTD as a Nonself RNA Recognition Domain

We found that CTD recognizes both dsRNA and 5′ppp ssRNA. CTD partially overlaps with RD and exhibits activity to bind with the helicase linker region (Figure 3E). Structural analysis by NMR spectroscopy revealed that CTD contains a surface enriched with basic amino acids as well as another surface with acidic patches. NMR titration by dsRNA and 5′ppp ssRNA revealed that these RNAs alter NMR signals derived from the basic surface, including the "basic cleft." Mutagenesis of full-length RIG-I confirmed that the basic surface is critical for the recognition of nonself RNA (Figures 6A–6D). It was surprising to find that a single

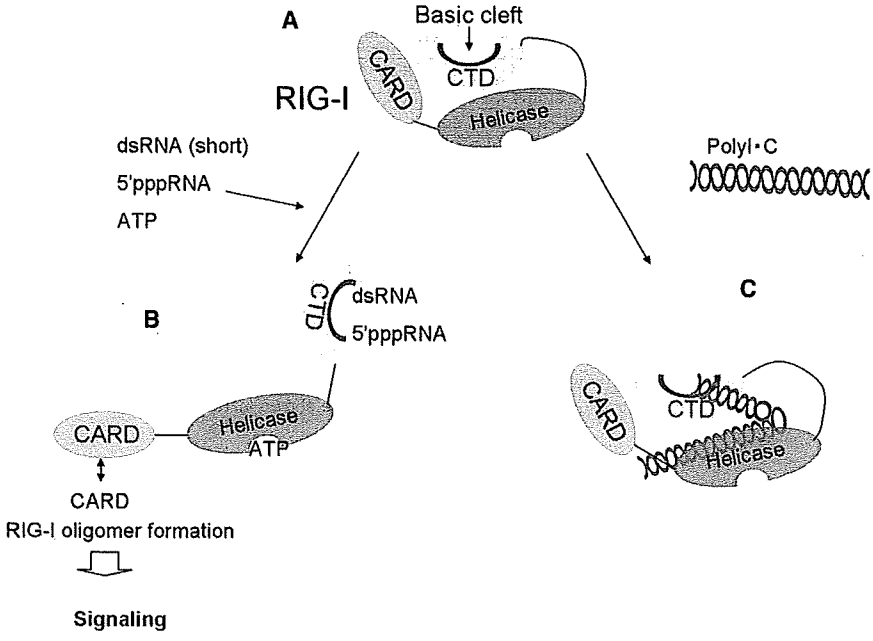

Figure 7. RIG-I Is Activated by Short dsRNA and 5′ppp ssRNA, but Not by Poly I:C

(A) Normally RIG-I conforms to closed structure, in which CARD function is repressed, presumably through interaction between CTD and helicase linker region.

(B) When viral infection occurs, short dsRNA or 5′ppp ssRNA is provided to activate RIG-I.

(C) Longer dsRNA such as poly I:C may interact with both CTD and helicase domain of RIG-I. This multipoint interaction allows formation of a stable complex inducing distinct conformation. See text for details.

domain structure is responsible for detecting rather discrete RNA structures. NMR spectra indicate that the loop between β5 and β6, which surrounds the cleft, is flexible (Figure S4), suggesting its involvement in the recognition of different RNA structures and/or conformational change induced by associating with nonself RNA. Interestingly, RIG-I KK878/880AA, which exhibits impaired binding to nonself RNA, is capable of binding with the helicase linker (our unpublished data). Furthermore, none of the mutations on the basic surface are constitutively active (Figures 6C and 6D), suggesting that RD's function may reside on the surface containing acidic patches. This is somewhat reminiscent of 2′-5′-oligoadenylate synthetase, which detects dsRNA by one surface with a basic cleft, and this interaction alters the catalytic domain on the opposite surface (Hartmann et al., 2003).

Analysis of cells derived from *RIG-I*$^{-/-}$ and *MDA5*$^{-/-}$ mice revealed that although poly I:C significantly binds to RIG-I in vitro, it is almost exclusively sensed by MDA5 (Gitlin et al., 2006; Kato et al., 2006). This apparent discrepancy in the binding activity and signaling capability of RIG-I could be partly explained by the observation that poly I:C requires an intact TAS motif in addition to CTD for binding (Figures 6E–6G), thus inducing a conformation distinct from that induced by dsRNA or 5′ppp ssRNA (Figure 3B and Figure S7).

Below is the current model for the activation of RIG-I (Figure 7). RIG-I conforms to a closed structure, in which CARD function is repressed, presumably through the interaction between CTD and the helicase linker region. When viral infection produces short dsRNA or 5′ppp-RNA and is bound to the basic cleft of CTD in the presence of ATP, RIG-I changes its conformation and releases CARD from the constraint. The released CARDs interact with each other to form RIG-I oligomers, relaying a signal through their interaction with IPS-1. When longer dsRNA, such as poly I:C, binds to RIG-I, interaction occurs with the helicase domain as well as with CTD. This multipoint interaction allows the formation of a stable complex, inducing distinct conformation. This complex is abortive, presumably due to its failure to expose CARD.

Poly I:C activates MDA5 in vivo, suggesting that MDA5 and RIG-I are activated differently. CTD of MDA5 is defective in dsRNA binding (Figure S10), and full-length MDA5 binds with poly I:C weakly (Yoneyama et al., 2005). Furthermore, CTD of LGP2 displays a strong binding activity to short dsRNA, but the corresponding region of MDA5 failed to do so. It is worth noting that lysine residue corresponding to K858 of RIG-I, which contributes to nonself RNA recognition (Figure S11), is conserved in LGP2 but is completely missing in MDA5 (Figure 4B). Therefore it is tempting to speculate that MDA5 functions in concert with other factors, such as LGP2.

EXPERIMENTAL PROCEDURES

Oligonucleotides

5′ppp ssRNA was synthesized by in vitro transcription using the T7 Megascript kit (Ambion, Austin, TX). Chemically synthesized RNAs were from Japan Bio Services Co., Ltd. (Saitama, Japan). For generating duplexes, RNA or DNA oligonucleotides were mixed in hybridization buffer (20 mM Tris-HCl [pH 8.0], 1.5 mM $MgCl_2$, and 1.5 mM DTT), boiled for 1 min, and incubated at 37°C for 1 hr. Where indicated, oligonucleotides were 5′ phosphorylated, or dephosphorylation was performed by T4 polynucleotide kinase or alkaline phosphatase (TaKaRa), respectively.

Binding Assay

Recombinant RIG-I proteins were mixed with oligonucleotides in a reaction mixture (10 μl, in hybridization buffer). After incubation at room temperature for 15 min, the reaction mixture was applied to a 7.5% acrylamide gel (Tris-glycin buffer) and stained with EtBr and CBB. When a radioactive probe was used, the mixture was applied to a 15% acrylamide gel (TBE buffer) and the radioactivity was detected with an Image Analyzer (Fuji). ^{32}P-poly I:C was prepared by labeling ~800 bp poly I:C isolated from agarose gel using T4 polynucleotide kinase and [γ-^{32}P]ATP.

Helicase Assay

^{32}P duplexes indicated in Figure S1 were prepared by annealing ^{32}P-25c or ^{32}P-D25c with appropriate complementary cold oligonucleotides. To prevent the reannealing of unwound duplexes, a 1000-fold molar excess of competitor (cold 25-mer oligonucleotide DNA or RNA complementary to ^{32}P-25c) was included in the mixture. The reaction mixture (10 μl), which contains 0.04 pmol ^{32}P-duplex substrate, 40 pmol competitor, 30 pmol recombinant RIG-I protein, 20 mM Tris-HCl (pH 8.0), 1.5 mM $MgCl_2$, 1.5 mM DTT, 70 mM KCl, 5 mM ATP or AMP-PNP, and 2 units/μl RNase Inhibitor (Roche), was incubated at 37°C for 60 min. The mixture was incubated at 37°C for 15 min and applied to a 7.5% SDS gel.

Plasmids

p-55C1BLuc, pRL-tk, and pEF-flagRIG-I were described previously (Yoneyama et al., 2004). The expression plasmids for RIG-I mutants, pEF-flagRIG-IR849A, pEF-flagRIG-IRK858/861AA, pEF-flagRIG-IRK878/880AA, and pEF-flagRIG-IKK888/907AA, were generated using a GeneEditor in vitro site-directed mutagenesis system (Promega).

Reporter Gene Assay

L929/C1B-Luc cells, stably integrating a reporter construct, p-55C1BLuc, were plated in 48-well plates, and treated with 10^3 units/ml mouse IFN-β for 15 hr and transfected with oligonucleotides using Trans-IT TKO (Invitrogen). After 12 hr, cell extracts were made and subjected to a luciferase assay. RIG-I KO MEFs (5×10^4) were transfected with p-55C1BLuc (0.7 μg), pRL-tk (7 ng), and expression plasmids for RIG-I mutants (1.4 μg) using FuGene6 transfection reagent (Roche). Cells were split into four aliquots, stimulated with RNA transfection for 12 hr, and harvested at 48 hr after DNA transfection.

IRF-3 Dimerization Assay

L929 cells or MEFs were plated in 3 cm dishes, treated with 10^3 units/ml mouse IFN-β for 12 hr, transfected with RNA using Trans-IT TKO, and cultured for 12 hr. Cell extracts were subjected to native PAGE and western blotting (Yoneyama et al., 2004).

Protease Digestion

The binding reaction mixture (10 μl) containing RIG-I (30 pmol) and oligonucleotides (10 pmol) was incubated at room temperature for 15 min. Proteases were added for digestion: trypsin (TPCK-treated trypsin, 0.16 μg, 37°C for 15 min, terminated by TLCK 1 μg/ml) and chymotrypsin (TLCK-treated chymotrypsin, 0.05 μg, 37°C for 30 min, terminated by TPCK 1 μg/ml). One-tenth of the digested RIG-I was analyzed by SDS-PAGE/immunoblotting using anti-human RIG-I monoclonal antibody (clone N3514, epitope: aa 218–792).

Recombinant Proteins

Production and purification of full-length RIG-I (1–925) were described elsewhere (Saito et al., 2007). The CTD (792–925) of human RIG-I was amplified by PCR and inserted into a pGEX-6P-1 vector to produce GST fusion protein (GE Healthcare). Expression vectors were introduced into *Escherichia coli* BL21(DE3) cells and cultured in M9 medium. Protein expression was induced by the addition of 1 mM IPTG when the absorbance at 600 nm was ~0.4. The cells were then grown at 16°C for 24 hr. The protein was purified with glutathione Sepharose 4B (GE Healthcare), then the GST was removed by PreScission protease (GE Healthcare). The protein was further purified with size-exclusion Superdex 75 columns (GE Healthcare). Uniformly labeled protein was expressed as described above, except for using medium containing ^{15}N-ammonium chloride and D-glucose (or 13C-D-glucose), and similarly purified. The NMR sample for structural determination was prepared at 0.5 mM in 50 mM Tris (pH 7), 250 mM NaCl, and 0.5 mM EDTA. The NMR sample for titration was further purified with Resource Q-Sepharose (GE Healthcare) to remove the residual nucleic acid and was prepared at 0.1 mM protein in 50 mM Tris (pH 7), 250 mM NaCl, and 1.5 mM DTT. Ten percent D2O was added to each sample for NMR lock.

293T cells (1×10^6 cells in 6 cm dish) were transfected with 20 μg of expression vector using calcium-phosphate method. At 48 hr after transfection, whole-cell extract was prepared (Yoneyama et al., 2004). The lysate was cleared by centrifugation (75,000 rpm, 10 min) and mixed with anti-Flag bead (Sigma) to adsorb Flag-tagged proteins. The bead was washed extensively, and bound protein was eluted with Flag peptide (Sigma).

For GST fusion proteins, Huh7 or 293T cells (5×10^5 cells in 6 cm dish) were transfected with 2 μg of expression vector using FuGene6 (Roche). At 24 hr after transfection, cell lysate was prepared (Yoneyama et al., 2004). The lysate was adsorbed to glutathione Sepharose 4B, and the GST fusion proteins were eluted with reduced glutathione.

NMR Measurements

NMR spectra were acquired at 15°C on Varian Unity Inova 600 and 800 spectrometers. Data were processed using NMRPipe (Delaglio et al., 1995) and analyzed using Sparky (http://www.cgl.ucsf.edu/home/sparky/). Backbone resonances were assigned using 3D HNCA, HN(CO)CA, HNCACB, CBCA(CO)NH, HNCO, HNCAHA, and HBHA(CO)NH spectra. Side-chain aliphatic atoms were assigned using 3D C(CO)NH, H(CCO)NH, CCH-TOCSY, and HCCH-TOCSY spectra, while aromatic side-chain atoms were assigned using 2D (Hb)Cb(CgCd)Hd, 3D CCH-TOCSY, and 3D HCCH-TOCSY spectra.

Structural Determination

3D ^{15}N-edited NOESY and ^{13}C-edited NOESY spectra (τ_{mix} = 100 ms) were measured to obtain the NOE distance constraints. Backbone ϕ and ψ dihedral angle constraints were generated using the program TALOS (Cornilescu et al., 1999). The structure of RIG-I CTD was determined using CANDID/CYANA 2.1 (Herrmann et al., 2002; Guntert et al., 1997). The best 20 structures were analyzed with PROCHECK-NMR (Laskowski et al., 1996). Structural statistics for RIG-I CTD are shown in Table 1.

NMR Titration

A chemical shift perturbation study of the amide nitrogen and proton signals of RIG-I CTD in ^{1}H-^{15}N HSQC spectra was performed with 5′ppp-GG25, GG25/2+25c, and ssRNAs GG25, 2+25 as control (Figure S1). Aliquots of RNA dissolved in water were added to ^{15}N-labeled RIG-I CTD at 0.1, 0.25, 0.5, 1.0, and 2.0 equivalents.

ACCESSION NUMBERS

The coordinates of the 20 lowest energy structures have been deposited in the Protein Data Bank under accession number 2RMJ.

SUPPLEMENTAL DATA

Supplemental Data include Supplemental Experimental Procedures, eleven figures, and one table and can be found with this article online at http://www.molecule.org/cgi/content/full/29/4/428/DC1/.

ACKNOWLEDGMENTS

We thank Dr. M. Horiuchi and Ms. Y. Fujioka for preparing RIG-I CTD. This work was supported by funds from the Ministry of Education, Culture, Sports, Science and Technology of Japan, Japan Society for the Promotion of Science, Nippon Boehringer Ingelheim Co., Ltd., and Mitsubishi Rayon Co., Ltd.

Received: June 18, 2007
Revised: October 1, 2007
Accepted: November 9, 2007
Published online: January 31, 2008

REFERENCES

Akira, S., Uematsu, S., and Takeuchi, O. (2006). Pathogen recognition and innate immunity. Cell *124*, 783–801.

Alexopoulou, L., Holt, A.C., Medzhitov, R., and Flavell, R.A. (2001). Recognition of double-stranded RNA and activation of NF-kappaB by Toll-like receptor 3. Nature *413*, 732–738.

Cordin, O., Banroques, J., Tanner, N.K., and Linder, P. (2006). The DEAD-box protein family of RNA helicases. Gene *367*, 17–37.

Cornilescu, G., Delaglio, F., and Bax, A. (1999). Protein backbone angle restraints from searching a database for chemical shift and sequence homology. J. Biomol. NMR *13*, 289–302.

Delaglio, F., Grzesiek, S., Vuister, G.W., Zhu, G., Pfeifer, J., and Bax, A. (1995). NMRPipe: a multidimensional spectral processing system based on UNIX pipes. J. Biomol. NMR *6*, 277–293.

Fujita, T. (2006). Virology. Sensing viral RNA amid your own. Science *314*, 935–936.

Gitlin, L., Barchet, W., Gilfillan, S., Cella, M., Beutler, B., Flavell, R.A., Diamond, M.S., and Colonna, M. (2006). Essential role of mda-5 in type I IFN responses to polyriboinosinic:polyribocytidylic acid and encephalomyocarditis picornavirus. Proc. Natl. Acad. Sci. USA *103*, 8459–8464.

Guntert, P., Mumenthaler, C., and Wuthrich, K. (1997). Torsion angle dynamics for NMR structure calculation with the new program DYANA. J. Mol. Biol. *273*, 283–298.

Hartmann, R., Justesen, J., Sarkar, S.N., Sen, G.C., and Yee, V.C. (2003). Crystal structure of the 2′-specific and double-stranded RNA-activated interferon-induced antiviral protein 2′-5′-oligoadenylate synthetase. Mol. Cell *12*, 1173–1185.

Herrmann, T., Guntert, P., and Wuthrich, K. (2002). Protein NMR structure determination with automated NOE assignment using the new software CANDID and the torsion angle dynamics algorithm DYANA. J. Mol. Biol. *319*, 209–227.

Holm, L., and Sander, C. (1993). Protein structure comparison by alignment of distance matrices. J. Mol. Biol. *233*, 123–138.

Hornung, V., Ellegast, J., Kim, S., Brzozka, K., Jung, A., Kato, H., Poeck, H., Akira, S., Conzelmann, K.K., Schlee, M., et al. (2006). 5′-triphosphate RNA is the ligand for RIG-I. Science *314*, 994–997.

Joklik, W.K. (1991). Interferons. In Fundamental Virology, Second Edition, B.N. Fields and D.M. Knipe, eds. (New York: Raven Press, Ltd.), pp. 343–370.

Kato, H., Sato, S., Yoneyama, M., Yamamoto, M., Uematsu, S., Matsui, K., Tsujimura, T., Takeda, K., Fujita, T., Takeuchi, O., and Akira, S. (2005). Cell type-specific involvement of RIG-I in antiviral response. Immunity *23*, 19–28.

Kato, H., Takeuchi, O., Sato, S., Yoneyama, M., Yamamoto, M., Matsui, K., Uematsu, S., Jung, A., Kawai, T., Ishii, K.J., et al. (2006). Differential roles of MDA5 and RIG-I helicases in the recognition of RNA viruses. Nature *441*, 101–105.

Laskowski, R.A., Rullmann, J.A., MacArthur, M.W., Kaptein, R., and Thornton, J.M. (1996). AQUA and PROCHECK-NMR: programs for checking the quality of protein structures solved by NMR. J. Biomol. NMR *8*, 477–486.

Marques, J.T., Devosse, T., Wang, D., Zamanian-Daryoush, M., Serbinowski, P., Hartmann, R., Fujita, T., Behlke, M.A., and Williams, B.R. (2006). A structural basis for discriminating between self and nonself double-stranded RNAs in mammalian cells. Nat. Biotechnol. *24*, 559–565.

Pause, A., and Sonenberg, N. (1992). Mutational analysis of a DEAD box RNA helicase: the mammalian translation initiation factor eIF-4A. EMBO J. *11*, 2643–2654.

Pichlmair, A., Schulz, O., Tan, C.P., Naslund, T.I., Liljestrom, P., Weber, F., and Reis e Sousa, C. (2006). RIG-I-mediated antiviral responses to single-stranded RNA bearing 5′-phosphates. Science *314*, 997–1001.

Rogers, G.W., Jr., Lima, W.F., and Merrick, W.C. (2001). Further characterization of the helicase activity of eIF4A. Substrate specificity. J. Biol. Chem. *276*, 12598–12608.

Saito, T., Hirai, R., Loo, Y.M., Owen, D., Johnson, C.L., Sinha, S.C., Akira, S., Fujita, T., and Gale, M., Jr. (2007). Regulation of innate antiviral defenses through a shared repressor domain in RIG-I and LGP2. Proc. Natl. Acad. Sci. USA *104*, 582–587.

Samuel, C.E. (2001). Antiviral actions of interferons. Clin. Microbiol. Rev. *14*, 778–809.

Yoneyama, M., and Fujita, T. (2007). Function of RIG-I-like receptors in antiviral innate immunity. J. Biol. Chem. *282*, 15315–15318.

Yoneyama, M., Kikuchi, M., Natsukawa, T., Shinobu, N., Imaizumi, T., Miyagishi, M., Taira, K., Akira, S., and Fujita, T. (2004). The RNA helicase RIG-I has an essential function in double-stranded RNA-induced innate antiviral responses. Nat. Immunol. *5*, 730–737.

Yoneyama, M., Kikuchi, M., Matsumoto, K., Imaizumi, T., Miyagishi, M., Taira, K., Foy, E., Loo, Y.M., Gale, M., Jr., Akira, S., et al. (2005). Shared and unique functions of the DExD/H-box helicases RIG-I, MDA5, and LGP2 in antiviral innate immunity. J. Immunol. *175*, 2851–2858.

Yu, H., and Schreiber, S.L. (1995a). Cloning, Zn2+ binding, and structural characterization of the guanine nucleotide exchange factor human Mss4. Biochemistry *34*, 9103–9110.

Yu, H., and Schreiber, S.L. (1995b). Structure of guanine-nucleotide-exchange factor human Mss4 and identification of its Rab-interacting surface. Nature *376*, 788–791.

Molecular Cell
Article

The C-Terminal Regulatory Domain Is the RNA 5′-Triphosphate Sensor of RIG-I

Sheng Cui,[1,2,6] Katharina Eisenächer,[4,6] Axel Kirchhofer,[1,2] Krzysztof Brzózka,[1,3] Alfred Lammens,[1,2] Katja Lammens,[1,2] Takashi Fujita,[5] Karl-Klaus Conzelmann,[1,3] Anne Krug,[4] and Karl-Peter Hopfner[1,2,*]
[1]Gene Center
[2]Center for Integrated Protein Science, Department of Chemistry and Biochemistry
[3]Max-von-Pettenkofer Institute
Ludwig-Maximilians-University of Munich, Feodor-Lynen-Strasse 25, 81377 Munich, Germany
[4]Department of Internal Medicine II, Technical University Munich, Ismaninger Strasse 22, 81675 Munich, Germany
[5]Department of Genetics and Molecular Biology, Institute for Virus Research, Kyoto University, Kyoto 606-8507, Japan
[6]These authors contributed equally to this work.
*Correspondence: hopfner@lmb.uni-muenchen.de
DOI 10.1016/j.molcel.2007.10.032

SUMMARY

The ATPase RIG-I senses viral RNAs that contain 5′-triphosphates in the cytoplasm. It initiates a signaling cascade that activates innate immune response by interferon and cytokine production, providing essential antiviral protection for the host. The mode of RNA 5′-triphosphate sensing by RIG-I remains elusive. We show that the C-terminal regulatory domain RD of RIG-I binds viral RNA in a 5′-triphosphate-dependent manner and activates the RIG-I ATPase by RNA-dependent dimerization. The crystal structure of RD reveals a zinc-binding domain that is structurally related to GDP/GTP exchange factors of Rab-like GTPases. The zinc coordination site is essential for RIG-I signaling and is also conserved in MDA5 and LGP2, suggesting related RD domains in all three enzymes. Structure-guided mutagenesis identifies a positively charged groove as likely 5′-triphosphate-binding site of RIG-I. This groove is distinct in MDA5 and LGP2, raising the possibility that RD confers ligand specificity.

INTRODUCTION

The innate immune system is a first line of defense against pathogen infection. The response to pathogens by the innate immune system of mammals is initiated by the detection of pathogen components by host pattern recognition receptors. These receptors specifically recognize molecules such as viral RNA and DNA, pathogen cell wall components, or flagellar proteins (Akira et al., 2006; Hiscott et al., 2006; Meylan et al., 2006). Viral RNA is recognized in the endosome by membrane-bound Toll-like receptors, or in the cytoplasm by retinoic acid inducible gene 1 (RIG-I, also known as DDX58) and melanoma differentiation associated antigen 5 (MDA5, also known as IFIH1 or Helicard) (Kawai and Akira, 2006; Seth et al., 2006). Upon recognition of cytosolic viral RNA, RIG-I and MDA5 bind to the adaptor protein IPS-1 (also known as CARDIF, MAVS, or VISA), which is located in the outer mitochondrial membrane (Kawai et al., 2005; Meylan et al., 2005; Seth et al., 2005; Xu et al., 2005). The interactions of RIG-I or MDA5 with IPS-1 initiate downstream signaling to interferon regulator factor 3 (IRF-3), IRF7, and NF-κB transcription factors, resulting in the antiviral response by interferon production and activation of interferon-stimulated genes as well as NF-κB target genes (Johnson and Gale, 2006).

RIG-I and MDA5 sense different types of viruses (Kato et al., 2006). RIG-I is a sensor for Hepatitis C virus, Sendai virus, influenza virus, vesicular stomatitis virus, rabies virus, and Japanese encephalitis virus, while MDA5 appears to detect only picornaviruses. Recent results show that RIG-I distinguishes viral RNA from the vast amount and variety of cellular RNAs by recognizing 5′-triphosphates, a modification that arises from RNA synthesis by many viruses but is not found on normal capped or processed cellular RNA (Hornung et al., 2006; Pichlmair et al., 2006; Plumet et al., 2007). Because the RIG-I stimulating HCV RNA is not known to contain 5′-pppRNA, nonphosphorylated dsRNA regions could also contribute to RIG-I activation. MDA5 activation can be stimulated by the dsRNA analog polyinosine-polycytidylic acid (poly[I:C]), but the precise determinants of viral RNA detected by MDA5 remain elusive (Gitlin et al., 2006). RIG-I and MDA5 are sequence related to a third protein, laboratory of genetics and physiology 2 (LGP2) (Yoneyama et al., 2005). The function of LGP2 in the innate immune system is less well understood, but it has been observed that expression of LGP2 interferes with the RIG-I-dependent stimulation of interferon production, suggesting it might have a regulatory role (Komuro and Horvath, 2006; Rothenfusser et al., 2005).

RIG-I, MDA5, and LGP2 belong to the superfamily 2 (SF2) helicases or ATPases (Gorbalenya et al., 1988; Hopfner and Michaelis, 2007). These enzymes share seven conserved sequence motifs (referred to as "helicase motifs") that mediate ATP and nucleic acid binding. ATP hydrolysis is typically stimulated by nucleic acid binding and results in a conformational powerstroke. SF2 helicases/ATPases can have diverse mechanistic functions, including separation of nucleic acid duplexes for bona fide helicases, translocation and motor function, or remodeling of nucleic acid structures or protein:nucleic acid complexes. Not all

of them, including RIG-I, MDA5, and LGP2, have been demonstrated to possess helicase activity, and the mechanistic role of ATP binding and hydrolysis to the DECH box domain of RIG-I is unclear.

Among SF2 ATPases, RIG-I, MDA5, and LGP2 possess a unique domain structure. RIG-I and MDA5 consist of two N-terminal caspase activation and recruitment domains (CARDs), a central SF2 type DECH box ATPase domain, and a C-terminal extension of little sequence homology to other proteins. LGP2 lacks the two N-terminal CARDs but contains the DECH box domain, as well as a C-terminal extension. The role of these domains in the function of RIG-I is only partly understood. Overexpression of the tandem CARDs of RIG-I can stimulate interferon production independently of the presence of viral RNA, suggesting that the CARDs mediate IPS-1 activation and downstream signaling (Yoneyama et al., 2004). Mutations in the ATP-binding site or truncation of parts of the DECH box domain abolish RIG-I activity, suggesting that ATP- and nucleic acid substrate-dependent conformational changes are a central part of viral RNA sensing (Hornung et al., 2006; Yoneyama et al., 2004). Recent results have shown that the C-terminal domain is required for RIG-I activity and that overexpression of the C-terminal domain inhibits RIG-I signaling in response to Sendai virus infections (Saito et al., 2007). Based on these findings, current models suggest that viral substrates induce an ATP-dependent conformational change that demasks the N-terminal CARDs for interaction with IPS-1. However, the mode of this activation and the nature of the 5′-triphosphate-binding site have not been revealed.

Here we report structural, biochemical, and in vivo analysis of the C-terminal regulatory domain (RD) of human RIG-I. Remarkably, RD contains a zinc-binding site and is structurally related to GDP/GTP exchange factors of Rab-like small GTPases. The zinc-binding site is essential for RIG-I signaling in vivo and is also conserved in MDA5 and LGP2, suggesting a similar activation principle underlying the function of the three DECH box enzymes. We demonstrate that 5′-triphosphate RNA binding to RD leads to dimerization of RIG-I and stimulation of the ATPase activity. Structure-guided mutagenesis identifies a conserved lysine at the bottom of a positively charged groove as likely recognition motif for RNA 5′-triphosphates. While fold and zinc coordination site are conserved, this lysine and other features of the recognition groove are different in LGP2 and MDA5, suggesting that RD could be a specificity determinant for different viral ligands.

RESULTS AND DISCUSSION

RD Activates and CARDs Inhibit RNA-Stimulated ATPase Activity of RIG-I In Vitro

To reveal domain functions in RNA-stimulated RIG-I activation, we analyzed the in vitro biochemical properties of human RIG-I together with a variety of truncation variants and isolated domains (Figure 1A). In particular, we tested RIG-I fragments that lack the two N-terminal CARDs (denoted "ΔCARD-RIG-I," residues 230–925), lack the C-terminal part that was recently described as repressor domain "RD" (denoted "RIG-I-ΔRD," residues 1–793), or lack both CARDs and RD and comprise the

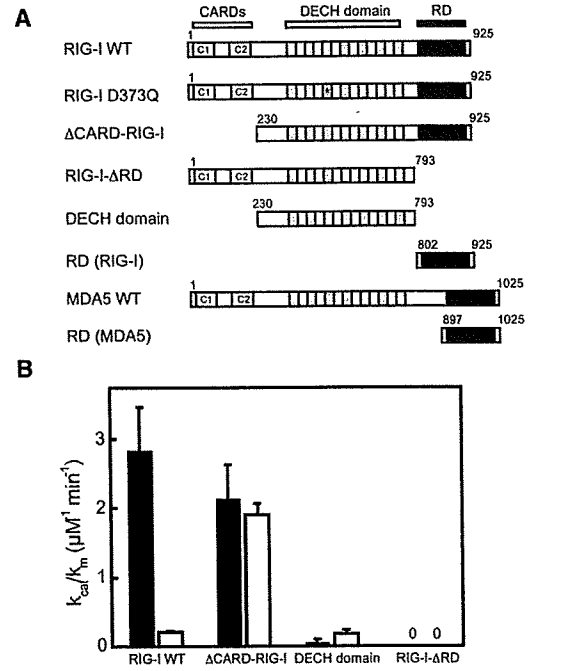

Figure 1. Biochemical Analysis of RIG-I Variants
(A) RIG-I and MDA5 variants used in this study.
(B) Catalytic efficiency (k_{cat} K_m^{-1}) of WT RIG-I and ΔCARD-RIG-I, RIG-I-ΔRD and the DECH domain for pppRVL (black bars), and nonphosphorylated dsRNA (white bars). Error bars represent standard errors of the nonlinear regression analysis (Supplemental Data).

DECH box ATPase domain (denoted "DECH domain," residues 230–793). We identified RD by a combination of limited proteolysis and secondary structure prediction. RD 742–925, similar to the recently published RD domain (Saito et al., 2007), tended to aggregate and was not suited for structural analysis in our hands. With RD 802–925 (denoted as "RD" in the following), we found a stable domain that was suitable for further structural studies.

We tested several RNA molecules for their ability to stimulate the ATPase activity of RIG-I and RIG-I variants in vitro: in vitro-transcribed 5′-triphosphate containing rabies virus leader RNA 58-mer (pppRVL) and 50-mers of nonphosphorylated synthetic ssRNA or dsRNA, corresponding to the sequence of the first 50 bases of RVL. We did not see significant ATPase activity for any RIG-I variants using synthetic ssRNA (see Figure S1 available online). However, pppRVL and synthetic dsRNA had the ability to activate the ATPase activity of RIG-I or some of its variants (Figure 1B). To reveal the efficiency of this activation and the activity of the various RIG-I variants, we measured k_{cat} and K_m values for the ATPase activities and calculated the catalytic efficiencies k_{cat}/K_m (Figure 1B, Figure S2, and Table S1).

We found that WT RIG-I is more efficiently activated by pppRVL than by the same amount of the dsRNA 50-mer. ΔCARD-RIG-I shows an only slightly reduced efficiency for pppRVL than WT RIG-I, indicating that the CARDs are not required for pppRVL stimulation of RIG-I. Remarkably, ΔCARD-RIG-I is much more efficiently stimulated by the nonphosphorylated dsRNA than WT RIG-I, and more or less equally

stimulated by dsRNA as by pppRVL. These results suggest that the CARDs appear to inhibit or block a dsRNA-binding site.

In contrast, a variant that lacks the RD domain was essentially inactive for all types of RNA assayed. This strong effect suggests that RD is required either for RNA binding or that it stimulates the ATPase activity of the DECH box domain by other means. To see whether RD is principally required for the ATPase activity of the DECH domain, we tested the isolated DECH domain for RNA-stimulated ATPase activity. Truncation of the CARDs from RIG-I-ΔRD, forming the isolated DECH domain, rescues some of the ATPase activity, which is now more efficiently stimulated by dsRNA than by pppRVL. This effect suggests that CARDs stabilize an inactive conformation, presumably by blocking an RNA-binding site on the DECH box domain, while RD is required to promote an active conformation of RIG-I in the presence of pppRVL. We do not know whether pppRVL can form local secondary structures or can form transient local duplexes, but the preferential activation of the DECH box domain by dsRNA indicates that in vivo signaling can also involve some sort of dsRNA regions.

The Regulatory Domain of RIG-I Recognizes 5′-Triphosphates

Because ΔCARD-RIG-I still responds to pppRVL and the DECH domain prefers dsRNA, it is unlikely that CARDs or the DECH domain contains the specificity site for RNA 5′-triphosphate recognition. We hypothesized that perhaps RD itself is the RNA 5′-triphosphate sensor of RIG-I. We analyzed the capability of RIG-I and RD to interact with pppRVL using fluorescence anisotropy analysis (Figure 2A). We observed binding isotherms for RIG-I that could be fitted to single site saturation curves. We used fluorescently labeled pppRVL, obtained by including a fluorescent uracil analog (Alexa Fluor 488-5-UTP) in the in vitro transcription reaction. RIG-I binds pppRVL with a K_d of 151 ± 8 nM. Much, but not all, of this binding affinity appears to reside in RD, because RD itself interacts with pppRVL with a K_d = 217 ± 11 nM. To see whether pppRVL recognition by RD depends on the 5′-triphosphate, we repeated the experiments with calf intestine alkaline phosphatase (CIAP)-treated RVL, which is devoid of the 5′-triphosphates. The integrity of the dephosphorylated RNA after CIAP treatment was verified by gel electrophoresis. In contrast to pppRVL, dephosphorylated RVL did not bind with significant affinity to RD. We also did not see significant binding of dsRNA (data not shown). Thus, RD binds to pppRVL in a 5′-triphosphate-dependent manner, suggesting it harbors the RNA 5′-triphosphate-binding site.

It has been previously observed that RD overexpression in cells inhibits RIG-I-dependent signaling in response to Sendai virus infections (Saito et al., 2007). The mechanism of this inhibition remained unclear. If RD binds the 5′-triphosphate, it could inhibit RIG-I by competing for pppRVL. To test this idea, we titrated RD into a solution containing ΔCARD-RIG-I (used because it more or less equally responds to pppRVL and dsRNA) and either pppRVL or nonphosphorylated dsRNA and measured residual ATPase activity. Adding increasing amounts of RD substantially reduced the capability of pppRVL to activate ΔCARD-RIG-I (Figure 2B and Table S2). A dose-dependent inhibition by RD of RIG-I downstream signaling was confirmed by reporter gene experiments in cell culture. Expression of increasing amounts of RIG-I RD domain from transfected plasmids reduced pppRVL-stimulated expression of IFN-β promoter-controlled

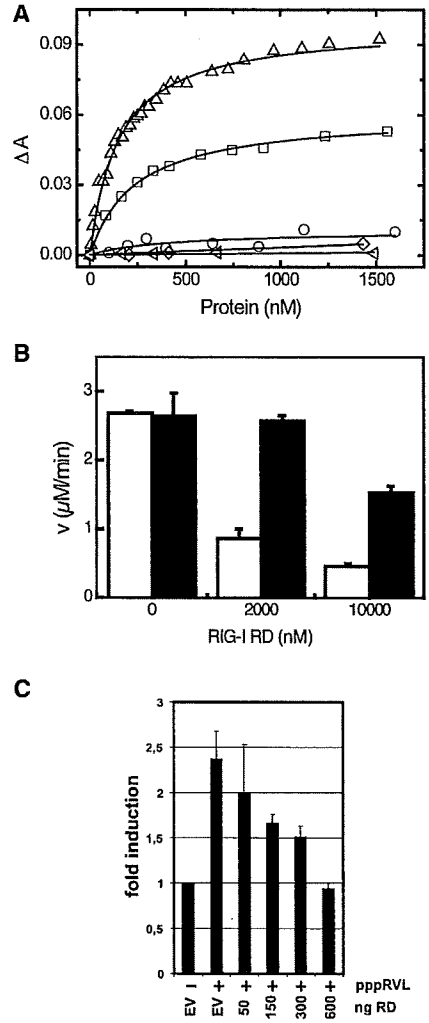

Figure 2. The RIG-I Regulatory Domain RD Binds RNA 5′-Triphosphates

(A) Fluorescence anisotropy changes (ΔA) measured by titrating WT RIG-I (△) or RD (□) into a solution containing fluorescently labeled pppRVL. Nonlinear regression against single site binding isotherms (solid lines) reveals dissociation constants of 151 ± 8 nM for WT RIG-I and 217 ± 11 nM for RD. Titration of RD into dephosphorylated RVL (○) or dsRNA (◁) did not result in significant changes in the anisotropy, suggesting that the 5′-triphosphate confers much of the binding affinity of pppRVL to RD. The RD of MDA5 (◇) also did not result in anisotropy changes for pppRVL.

(B) Dose-dependent inhibition of the ATPase activity of 20 nM ΔCARD-RIG-I by adding indicated amounts of RD in the presence of 200 nM pppRVL (white bars) or 200 nM dsRNA (black bars). Data represent mean and standard deviations (error bars) of three independent measurements.

(C) Dose-dependent inhibition of RIG-I-dependent activation of the IFN-β promoter. 293T cells were transfected with the indicated amounts of plasmids encoding RIG-I-RD or empty plasmid vector (EV) along with 100 ng of WT RIG-I plasmid. Activation of IFN-β promoter-controlled firefly luciferase (p125-FF-Luc) after transfection of 200 ng of pppRVL was determined in the Dual Luciferase Reporter System. Data represent mean and standard deviations (error bars) of three independent measurements.

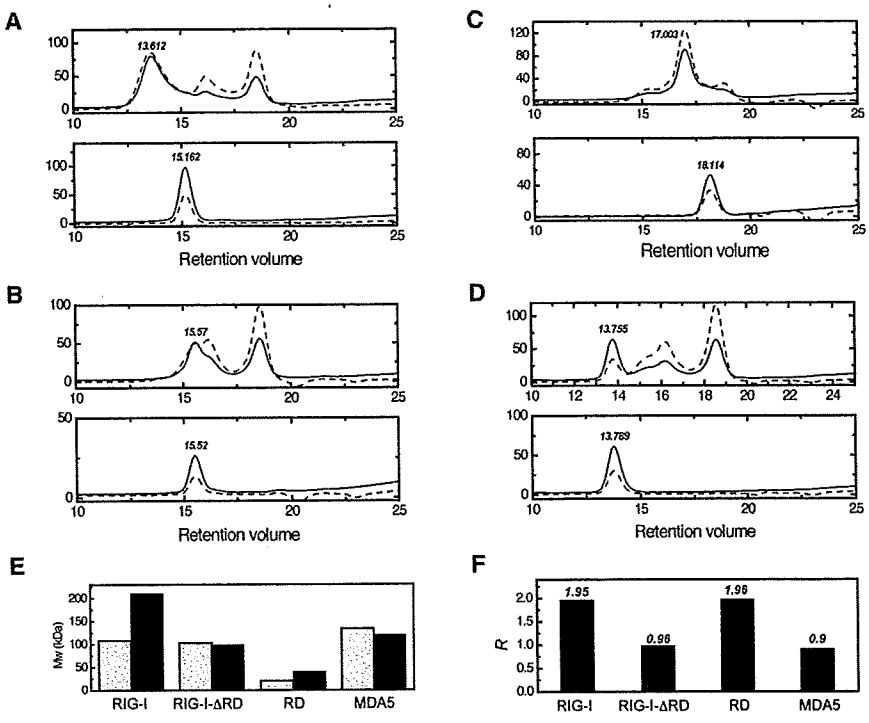

Figure 3. RD Promotes pppRVL-Dependent RIG-I Dimerization

Gel filtration analysis of pppRVL-dependent dimerization of RIG-I (A), RIG-I-ΔRD (B), RD (C), and MDA5 (D) in the presence (upper panels) and absence (lower panels) of pppRVL. Plotted are UV absorption profiles (260 nm, dashed lines; 280 nm, solid lines). The retention volume maxima of the proteins (verified by gel electrophoresis) are indicated. Additional peaks with increased 260 nm over 280 nm absorption stem from free RNA. The molecular weight of the protein fractions was analyzed by light scattering (E) and plotted as relative (*R*) value compared to the calculated monomer weights (F). RIG-I and RD form dimers in the presence of pppRVL while RIG-I-ΔRD and MDA5 are still monomeric, indicating that RIG-I RD promotes specific pppRVL dimer formation of RIG-I.

luciferase assay (Figure 2C). However, we also observe that RD interferes somewhat with the ability of dsRNA to activate ΔCARD-RIG-I, albeit at a much lower level (Figure 2B and Table S2). These effects could be explained if RD has two properties. The much more robust inhibition of pppRVL stimulation than dsRNA stimulation could be explained by competition for pppRVL. The additional weaker inhibition of dsRNA stimulation could be explained if the separately added RD interferes with the activation of the DECH box domain, for instance by interfering with proper multimer formation of RIG-I (see below and Saito et al. [2007]).

pppRVL Binding to RD Dimerizes RIG-I

It has been previously observed that RIG-I activation in cells includes some form of multimer formation that depends on RD (Saito et al., 2007). Thus, we tested whether RD itself is a 5′-triphosphate-dependent multimerization domain and studied the multimerization properties of RIG-I variants along with MDA5 as control by gel filtration and light scattering (Figure 3). In the absence of pppRVL, RIG-I and RIG-I-ΔRD as well as MDA5 are monomeric with apparent molecular weights of 115 kDa, 103 kDa, and 135 kDa. These values match, within the resolution of the experimental method, the expected calculated molecular weights of 109 kDa, 93 kDa, and 118 kDa of monomeric RIG-I, RIG-I-ΔRD, and MDA5. Slightly higher measured molecular weights often indicate nonspherical molecular shapes.

Upon preincubation with pppRVL, RIG-I forms dimers, inferred from apparent molecular weights of 210 kDa. In contrast, MDA and RIG-I-ΔRD still eluted as monomers, with apparent molecular weights of 121 kDa and 99 kDa, indicating that RD of RIG-I is required for pppRVL-dependent dimer formation of RIG-I. This dimer formation is RNA 5′-triphosphate dependent, because synthetic ssRNA 50-mer was unable to induce dimer formation of RIG-I (Figure S3).

We then tested whether RD itself can form dimers and whether this process depends on RNA 5′-triphosphates. In the absence of pppRVL, RD eluted as monomer (21 kDa), while in the presence of pppRVL we observed a molecular weight of 40 kDa. This value is in between the value for an RD dimer (expected MW 34 kDa) and a trimer composed of RD plus one pppRVL (expected MW 53 kDA). One possible explanation for this intermediate value is that the complex transiently dissociates and thus runs at a lower apparent molecular weight. NTPs and nonphosphorylated synthetic ssRNA did not change the elution profile of monomeric RD (Figure S3).

In conjunction with the ATPase and pppRVL binding data (Figures 1 and 2), our results suggest a dual mechanistic role for RD. On one side, it is a recognition domain for RNA 5′-triphosphates; on the other side, it triggers a structural switch that dimerizes RIG-I. Such a dual role also provides an explanation for the observation that RD is not only involved in RIG-I activation by pppRVL but also by dsRNA in vitro (Figure 1B). For instance, if the ATPase activity is stimulated by dimer formation, a lack of dimer formation in RIG-I-ΔRD constructs could reduce ATPase activity for all types of RNA, including dsRNA.

Crystallization and Structural Analysis of RD

To derive a structural framework for this multifunctional role of RD in RIG-I regulation, we crystallized RD and determined the crystal structure to 2.7 Å resolution. We noticed that RD contains several invariant cysteine residues and hypothesized that this region could form a metal-binding site. In fact, our crystals grew in the presence of zinc. To obtain phases, we replaced zinc with mercury by soaking the crystals in a solution that contains Hg-acetate and collected multiple anomalous dispersion data at the mercury L_{III} absorption edge. The resulting electron density allowed us to build all ten RD molecules in the asymmetric unit (Figure 4A and Table 1). We also determined a 3.0 Å crystal